



Politechnika Łódzka



POLITECHNIKA ŁÓDZKA

Wydział Elektrotechniki, Elektroniki, Informatyki i Automatyki Politechniki Łódzkiej

Praca Dyplomowa Magisterska

**Cyfrowe przetwarzanie impulsów z detektorów
promieniowania w czasie rzeczywistym z
wykorzystaniem układów programowalnych FPGA**

**Real Time Digital Pulse Processing from Radiation
Detectors Using Field Programmable Gate Arrays**

inż. Wojciech Mateusz Walewski

Nr albumu: 239587

Promotor:

dr hab. inż. Dariusz Makowski, prof. uczelnii

6 sierpnia 2022

Contents

1	Introduction	6
1.1	Motivation	6
1.2	Fission energy	7
1.3	Fusion energy	8
1.4	ITER Tokamak Project	10
1.4.1	Tokamak	10
1.4.2	ITER Goals	11
1.5	Real time diagnostics	12
1.5.1	Field Programmable Gate Arrays	13
1.6	Problem statement	14
2	Hard X-Ray spectroscopy	15
2.1	Runaway electrons	15
2.2	PhotoMultiplier Tubes	16
2.3	Preamplifiers	17
2.4	Pulse processing chains	17
2.4.1	Analogue processing chains	18
2.4.2	Digital processing chains	18
2.5	ITER HXRM specification	19
3	Research setup	21
3.1	PMT	21
3.2	Preamplifier	21
3.3	Digitizer board	21

3.3.1	Open FPGA design	23
3.3.2	Parallel sampling	23
3.4	Host computer	24
3.5	Software package	24
4	Pulse detection	25
4.1	Level trigger	25
4.2	Boxcar filter	27
4.3	Trapezoidal filter	29
4.4	Triangular filter	32
4.5	Other pulse detection methods	33
4.6	Simulation performance	33
5	Pulse Height Analysis	36
5.1	Pulse shaping algorithms	36
5.2	Integration	36
5.3	Simulated performance	37
6	HXR_M firmware	38
6.1	System overview	38
6.2	System control	39
6.3	Pulse detection	39
6.4	Pulse height analysis	42
6.5	Spectrum storage and transfer	43
7	Data transfer	45

7.1	PCIe interface	45
7.2	Direct memory access	45
7.3	Data pathways in the system	45
7.4	Multi-threaded data transfer	45
7.5	Software optimization	45
8	Conclusions	46
8.1	Further problems	46
8.2	Future research	46

Streszczenie

 Lorem ipsum dolor sit amet, consectetuer adipiscing elit. Ut purus elit, vestibulum ut, placerat ac, adipiscing vitae, felis. Curabitur dictum gravida mauris. Nam arcu libero, nonummy eget, consectetuer id, vulputate a, magna. Donec vehicula augue eu neque. Pellentesque habitant morbi tristique senectus et netus et malesuada fames ac turpis egestas. Mauris ut leo. Cras viverra metus rhoncus sem. Nulla et lectus vestibulum urna fringilla ultrices. Phasellus eu tellus sit amet tortor gravida placerat. Integer sapien est, iaculis in, pretium quis, viverra ac, nunc. Praesent eget sem vel leo ultrices bibendum. Aenean faucibus. Morbi dolor nulla, malesuada eu, pulvinar at, mollis ac, nulla. Curabitur auctor semper nulla. Donec varius orci eget risus. Duis nibh mi, congue eu, accumsan eleifend, sagittis quis, diam. Duis eget orci sit amet orci dignissim rutrum.

 Nam dui ligula, fringilla a, euismod sodales, sollicitudin vel, wisi. Morbi auctor lorem non justo. Nam lacus libero, pretium at, lobortis vitae, ultricies et, tellus. Donec aliquet, tortor sed accumsan bibendum, erat ligula aliquet magna, vitae ornare odio metus a mi. Morbi ac orci et nisl hendrerit mollis. Suspendisse ut massa. Cras nec ante. Pellentesque a nulla. Cum sociis natoque penatibus et magnis dis parturient montes, nascetur ridiculus mus. Aliquam tincidunt urna. Nulla ullamcorper vestibulum turpis. Pellentesque cursus luctus mauris.

 Nulla malesuada porttitor diam. Donec felis erat, congue non, volutpat at, tincidunt tristique, libero. Vivamus viverra fermentum felis. Donec nonummy pellentesque ante. Phasellus adipiscing semper elit. Proin fermentum massa ac quam. Sed diam turpis, molestie vitae, placerat a, molestie nec, leo. Maecenas lacinia. Nam ipsum ligula, eleifend at, accumsan nec, suscipit a, ipsum. Morbi blandit ligula feugiat magna. Nunc eleifend consequat lorem. Sed lacinia nulla vitae enim. Pellentesque tincidunt purus vel magna. Integer non enim. Praesent euismod nunc eu purus. Donec bibendum quam in tellus. Nullam cursus pulvinar lectus. Donec et mi. Nam vulputate metus eu enim. Vestibulum pellentesque felis eu massa.

Abstract

Nulla malesuada porttitor diam. Donec felis erat, congue non, volutpat at, tincidunt tristique, libero. Vivamus viverra fermentum felis. Donec nonummy pellentesque ante. Phasellus adipiscing semper elit. Proin fermentum massa ac quam. Sed diam turpis, molestie vitae, placerat a, molestie nec, leo. Maecenas lacinia. Nam ipsum ligula, eleifend at, accumsan nec, suscipit a, ipsum. Morbi blandit ligula feugiat magna. Nunc eleifend consequat lorem. Sed lacinia nulla vitae enim. Pellentesque tincidunt purus vel magna. Integer non enim. Praesent euismod nunc eu purus. Donec bibendum quam in tellus. Nullam cursus pulvinar lectus. Donec et mi. Nam vulputate metus eu enim. Vestibulum pellentesque felis eu massa.

Quisque ullamcorper placerat ipsum. Cras nibh. Morbi vel justo vitae lacus tincidunt ultrices. Lorem ipsum dolor sit amet, consectetur adipiscing elit. In hac habitasse platea dictumst. Integer tempus convallis augue. Etiam facilisis. Nunc elementum fermentum wisi. Aenean placerat. Ut imperdiet, enim sed gravida sollicitudin, felis odio placerat quam, ac pulvinar elit purus eget enim. Nunc vitae tortor. Proin tempus nibh sit amet nisl. Vivamus quis tortor vitae risus porta vehicula.

Fusce mauris. Vestibulum luctus nibh at lectus. Sed bibendum, nulla a faucibus semper, leo velit ultricies tellus, ac venenatis arcu wisi vel nisl. Vestibulum diam. Aliquam pellentesque, augue quis sagittis posuere, turpis lacus congue quam, in hendrerit risus eros eget felis. Maecenas eget erat in sapien mattis porttitor. Vestibulum porttitor. Nulla facilisi. Sed a turpis eu lacus commodo facilisis. Morbi fringilla, wisi in dignissim interdum, justo lectus sagittis dui, et vehicula libero dui cursus dui. Mauris tempor ligula sed lacus. Duis cursus enim ut augue. Cras ac magna. Cras nulla. Nulla egestas. Curabitur a leo. Quisque egestas wisi eget nunc. Nam feugiat lacus vel est. Curabitur consectetur.

1 Introduction

1.1 Motivation

Concerns regarding the sustainability of using fossil fuels for energy generation have been raised as early as the 1970s [1]. One of the most well-known examples from that time was the 1972 report titled "Limits to Growth" by Meadows et. al. [2]. In it a group of MIT scientists attempted to answer the question of how long will the Earth's natural resources last for considering the seemingly neverending growth of human civilisation. As a result of a conducted computer simulation, a rough estimate of around 100 years was given as a timeframe, after which the population would start to collapse due to a lack of resources.

This estimate did not go without controversies back when it was first published. The methodology was thoroughly picked apart, leading many to dismiss the study findings [1]. Naturally, nowadays, we are much better poised to verify the claims made by the now 50 year old book. The impeding resource depletion has certainly been made a less valid claim as technological progress made it possible to locate and tap into previously inaccessible fossil fuel fields [3]. Taking into account other issues, however, the original timeline of 100 years might have actually shifted closer.

When it comes to fossil fuel usage, in the last twenty years, the primary concerns have changed from resource depletion to global warming and irreversible environmental damage [1]. In 2018 the Intergovernmental Panel on Climate Change (IPCC) published a report indicating the need to stop the global temperature increase at 1.5°C above the levels measurable in the pre-industrial era. Failure to do so is projected to lead to irreversible climate changes and in turn serious damage to human settlements around the world. [4]

Fossil fuels account for as much as 70% of greenhouse gas emissions. Electricity generation alone causes 25-35% [5] of the total amount. Such a high share means that reducing this output is going to be crucial in meeting the goals outlined by the IPCC. At the beginning of the twentieth century, renewable energies, i.e. wind, solar, biomass and geothermal were thought to be the perfect solution to the issue at hand [6].

In modern times, we have now become aware of multiple issues that make renewable energy generation a problem at large scale. Most importantly, their efficacy varies depending on the geographical location and climate. Even when placed in optimal condi-

tions, they do not offer perfect stability. Additionally, the land usage is greater than the traditional forms of energy production [7].

1.2 Fission energy

The drawbacks of renewable energies have led to a formation of an alternative approach in both research and policymaking. The use of nuclear energy for supplementing the shortcomings of renewables has been suggested as a potential path forward. This concept is referred to as hybrid nuclear-renewable system. [8].

There are two ways that nuclear energy can be created and harnessed. In the more well-established technology, fission, heavy atoms (usually Uranium) are bombarded with neutrons and split into two or more lighter nuclei and additional neutrons as shown in Figure 1. The reaction is self-sustaining and releases energy in the form of heat that is then used to boil water. The steam causes turbines to spin and generate electricity.

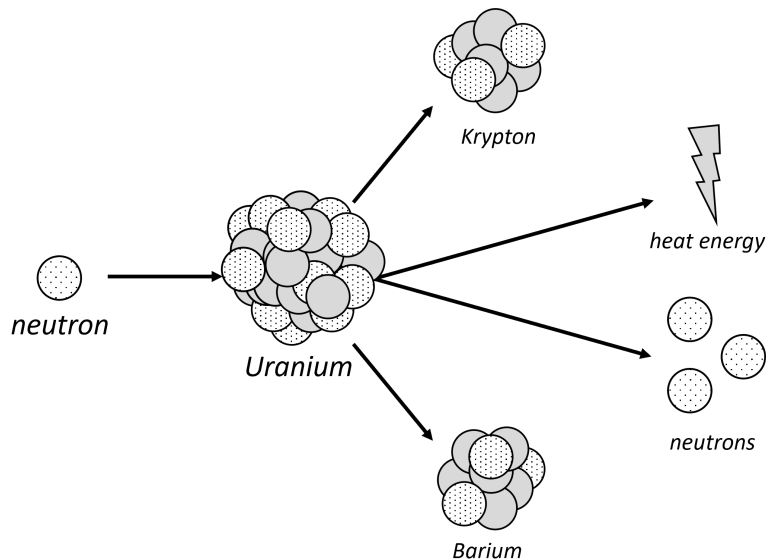


Figure 1: Uranium fission reaction

Fission is far from a new concept, as first fission reactors have been built as early as 1942 [9]. Although the technology itself is quite old and has been greatly improved over time, there is reasonable reluctance to build and use fission power plants. The issue that gets raised most often is the storage of radioactive waste. There are, however, multiple less well-known problems with fission [10].

The tragedies of Chornobyl and Fukushima reactors have caused many people to be wary of fission. However, even if democratic support is disregarded in policymaking, the acquisition, storage and disposal of radioactive materials required for and produced during fission prove to be an administrative challenge, especially if reactor construction and maintenance is to be handled by private entities [11]. The complexity of the problem suggests that as we arrive to more concrete solutions we should not stop exploring other potential alternatives.

1.3 Fusion energy

Just like it is possible to split atoms, it is also possible to combine them together in a process referred to as fusion. Fusing atoms lighter than Iron is a reaction that can produce surplus energy as highlighted by Figure 2. Two atoms of low binding energy can fuse into an atom of higher binding energy, releasing heat based on the mass-energy equivalence formula. The output energy can be used to generate electricity in the exact same manner as with fission. The problem with fusion reactors is that the conditions necessary for fusion to happen are extremely harder to achieve and sustain [12].

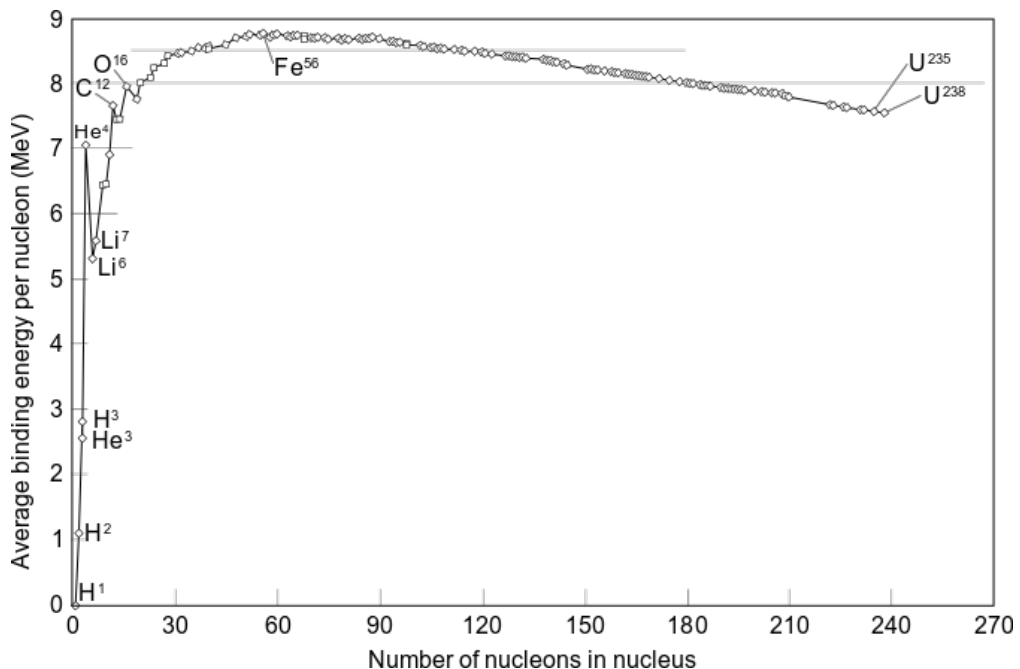


Figure 2: Average binding energy per nucleon as a function of the number of nucleons in the atom

Fusion is the primary reaction that causes stars to emit light and heat. The reaction that is most often artificially attempted on Earth differs from that occurring naturally in the

Sun. There, a p-p reaction occurs. This means the need of converting 4 protons into ${}^4\text{He}$. Replicating this reaction on a larger scale is extremely challenging due to the need to convert protons into neutrons. On Earth, fusion experiments primarily rely on using hydrogen isotopes, most commonly deuterium (D) and tritium (T) shown in Figure 3.

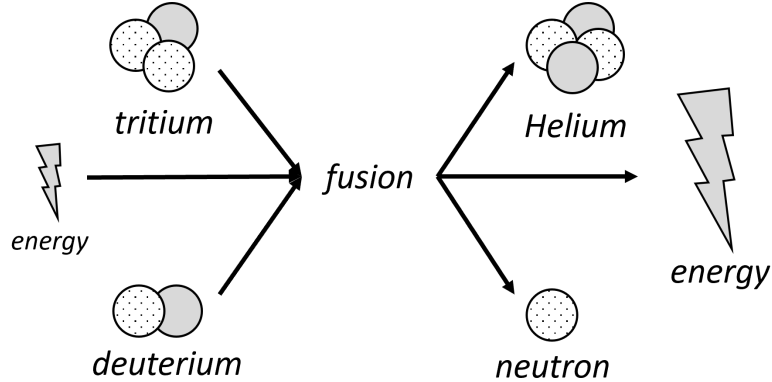


Figure 3: D-T fusion reaction

Despite being an easier approach, it still requires us to sustain a 200 million °C plasma. This means that an enormous amount of energy must be used to first heat the plasma up and then confine it to prevent it from completely destroying the reactor. The efficiency of D-T reactions might, however, worth the trouble. Theoretically, just 30 mg of deuterium would generate as much energy as 250 l of gasoline [13].

Such numbers sound incredible, but there are naturally multiple drawbacks too. Tritium, the other input material of this most promising reaction is extremely rare in nature. Its artificial production is currently done only by a select number of facilities. Combined with its relatively short half-life of around 12 years, there are fears of it running out. It is proven that fusion reactors will be capable of "breeding" their own tritium, however the transition period may still prove to be troublesome [14].

In the end, despite being a similarly old technology as fission [15], a fusion reactor with a net positive energy balance has not yet been constructed. Containing plasma heated to such extreme temperatures cannot be achieved with any solid material and must be done with the use of inertial or magnetic forces. The most common reactors that employ this concept are: tokamaks (Figure 4) and stellarators (Figure 5). The former design has been selected for probably the most ambitious fusion project to date, the International Thermonuclear Experimental Reactor (ITER) [13].

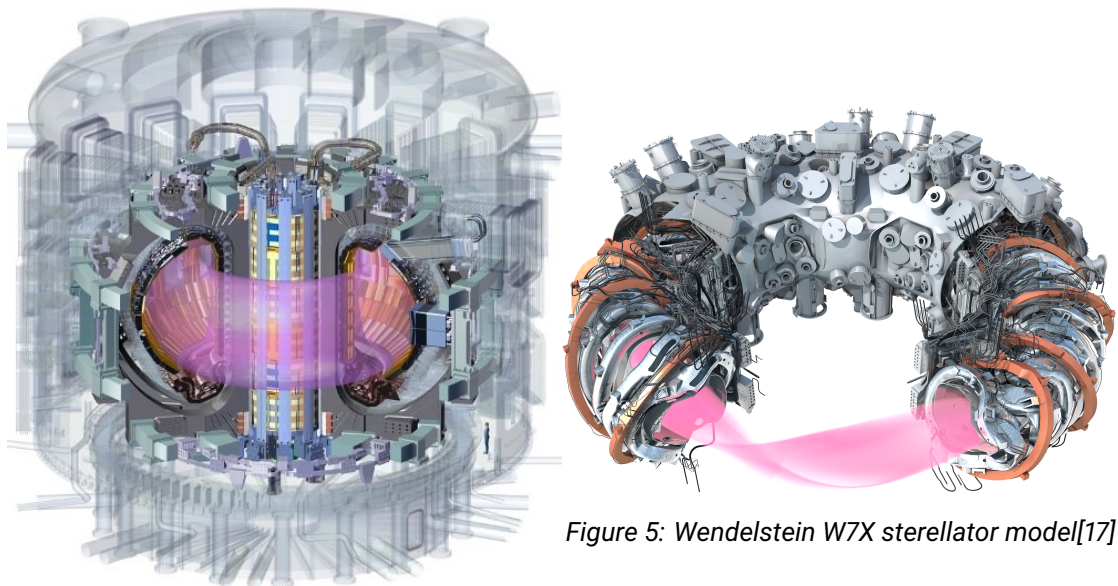


Figure 5: Wendelstein W7X stellarator model[17]

Figure 4: ITER tokamak model[16]

1.4 ITER Tokamak Project

1.4.1 Tokamak

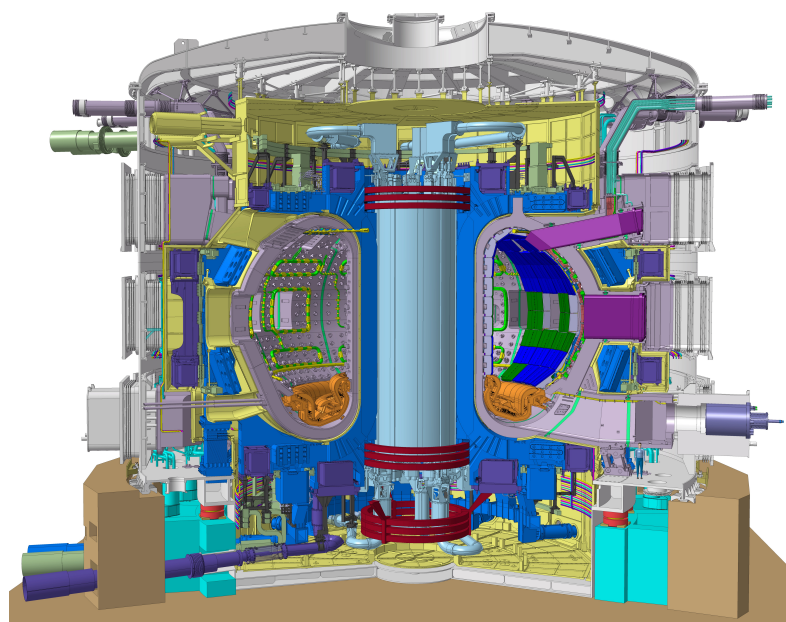


Figure 6: ITER tokamak cross section[16]

Tokamaks are reactors composed of a toroidal vacuum chamber surrounded by massive electromagnetic coils as shown in Figure 6. The magnetic fields are used to shape plasma and keep it away from the device internal walls. Operation starts with the removal of air and impurities from the vessel. The gaseous fuel is introduced and a strong current is induced ionizing the gases, thus forming plasma. Additional heat is introduced with microwave and fuel injections. Particles within the formed plasma can then collide with such force that they begin to break through atomic repulsion and fuse producing a large amount of energy. [16]

1.4.2 ITER Goals

At 24 m height and 30 m width, ITER will be the biggest tokamak ever constructed. That's twice as big as the largest experimental reactor currently in service, the Joint European Torus (JET). JET has been working since 1983 with a goal of achieving net energy gain. Despite running successful plasma experiments and recently starting deuterium-tritium experiments, the highest fusion energy gain Q (the ratio of produced power to the power required to sustain the plasma) obtained by JET was 0.33. A record only recently topped by a different type of a fusion device held at the US Department of Energy's National Ignition Facility. Using laser technology it was possible to obtain a Q of 0.7 for 4 billionths of a second. [18]

Although not supposed to work as a power plant, just an experiment, throughout its operation ITER intends to break this record by a lot. The new reactor is designed to reach an energy gain of 10 for the duration of a few minutes. This is of course still a theoretical plan, as the facility is still a fairly long time from being finished. As of 2022, the vacuum vessel is yet to be welded together[19]. First plasma operation is scheduled for the end of 2025[19], although multiple delays have already happened in the past [20], so future ones would at this point not be too surprising. Figure 7 shows an aerial picture of ITER from 14th of April 2020. Not all facilities have been fully constructed at this time.



Figure 7: Aerial view of the ITER facility as of 2022[16]

1.5 Real time diagnostics

With a project of such large magnitude as ITER it is near impossible to predict everything that might go wrong. There are naturally safety concerns, questions regarding the ambitious goals set by the management and the troubles of international cooperation[20]. It is thus crucial to maintain maximum operational safety and log all experimental data. This should ensure that even in the case of partial failure of the project important practical knowledge can be recorded for future fusion experiments.

When operational, ITER will rely on around 50 completely different measurement systems to control, evaluate and investigate its plasma [21]. This translates into dozens of gigabytes of data being generated, processed and archived every second as the experiment is running [22]. With some of the experiments lasting fractions of a second, a lot of the critical data acquisition and control must occur in real time and without waiting for human reaction [23]. This poses an important challenge when it comes to the choice of computing apparatus. A perfect device would offer infinite configurability preferably with remote access as well as a very high data throughput.

Traditional computers or more precisely Central Processing Units (CPUs) are remotely reprogrammable but may offer insufficient speeds in some of the real time applications. On the other end of this scale lie Application Specific Integrated Circuits (ASIC). These devices are an arrangement of digital logic gates realizing one specific goal, like digital signal filtering or processing network packets. ASICs offer unmatched bandwidth but cannot really be reconfigured after deployment, making them a risky choice in highly

experimental applications such as tokamaks.

1.5.1 Field Programmable Gate Arrays

Devices that offer a compromise between speed and reconfigurability exist nowadays. Most commonly Field Programmable Gate Arrays (FPGAs) are used. FPGAs are formed out of matrices of so called Configurable Logic Blocks (CLBs). These are small circuits that produce a single bit of logic output out of 4 input bits, using a reprogrammable function. These blocks are then wired together using programmable interconnects. Such design allows for the implementation of very efficient digital algorithms directly with the use of logical gates, without the need for an entire processor. [24]

The interconnects and CLB internal structure introduce additional wiring that would be unnecessary in the case of ASICs. These stray capacitances and inductances limit the maximum clock speed of FPGAs. This is not too much of an issue provided that the function can be parallelised. To offset this limitation, most FPGAs manufactured today come packed with more complex sub-circuitry that can be intermixed with the CLBs as indicated in Figure 8. These components can vary greatly from fast arithmetical blocks to small CPU-based microcontrollers.

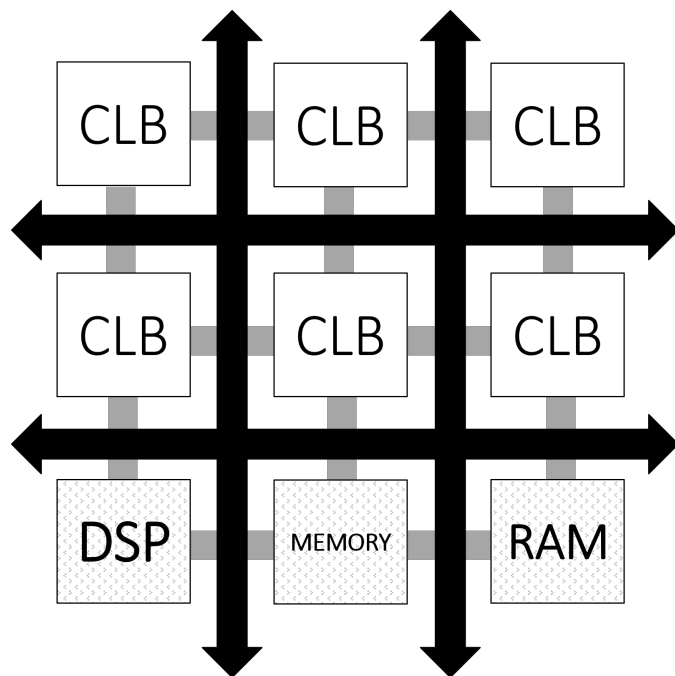


Figure 8: The internal structure of an FPGA

1.6 Problem statement

The nature of FPGAs makes them instrumental in the data acquisition and control systems of modern fusion experiments like the ITER tokamak. This work evaluates the potential usage of Field Programmable Gate Arrays for the detection and analysis of pulses produced by PhotoMultiplier Tubes (PMTs) being part of a High X-Ray Monitor (HXRM) designed to monitor Runaway Electrons (REs) at tokamaks.

A functional system for the Digital Pulse Processing (DPP) at the rate of 1 GS/s is proposed and implemented in an FPGA. A custom software package for control and data acquisition is shown. The optimization of both hardware and software is described. Different algorithms for pulse detection and discrimination are analysed, simulated and implemented in hardware. Finally design considerations for future systems are given.

2 Hard X-Ray spectroscopy

One of the diagnostic systems present in most of currently existing tokamaks is the Hard X-Ray Monitor (HXRM). It will also be used in ITER. The device is tasked with measuring the spectrum of X-Ray radiation inside the fusion vessel. The presence of high energy X-Ray radiation can point to problems with the plasma stability and suggest the need for mitigation techniques. [25]

2.1 Runaway electrons

The plasma in a tokamak is heated to a level where particles reach a velocity enabling them to break through atomic repulsion. In such conditions some particles can also obtain sufficient speed to escape the magnetic confinement of the vessel. Typically collisions with other particles are so frequent that in stable plasma these disturbances are not happening in large quantities. Directly after plasma is disrupted or terminated, the probability of collisions is lessened and a tokamak might start acting like a particle accelerator, bringing the electrons to nearly the speed of light. Electrons that act in this manner are called Runaway Electrons (REs). [26]

This phenomenon can occur in the form of a high-energy concentrated beam capable of melting the front-facing walls of a reactor. The effects of such damage being purposefully introduced in the JET tokamak are shown in Figure 9. To prevent mitigate the destructive effects of REs their generation has to be avoided if possible. Otherwise they must be detected and dealt with accordingly. Typically plasma heating might be reduced, or the electromagnets are precisely accentuated to reduce the disruptions. More extreme methods might involve the injection of noble gases in a process called Massive Gas Injection (MGI) [27].



Figure 9: Effects of RE in the JET vessel[26]

When REs interact with the Plasma Facing Components (PFCs) they lose their energy and emit X-Ray radiation in the Bremsstrahlung process. The energy of this radiation varies greatly, ranging from tens of keV (Soft X-Ray) to multiple MeV (Hard X-Ray). [28]

2.2 PhotoMultiplier Tubes

The photons generated in Bremsstrahlung by Runaway Electrons can be detected with the use of a device known as a PhotoMultiplier Tube (PMT). A PMT is built with the use of a photocathode and an electron multiplier. When a radiation photon hits the photocathode an electron is emitted due to the photoelectric effect. The electric fields in a PMT accelerate the electron towards a series of dynodes. Each collision with a dynode causes a release of additional electrons and forms a stronger beam that eventually reaches the anode where it becomes measurable as a current pulse. Figure 10 shows the internal structure of a PMT together with the output signal, a sharp exponentially decaying current pulse. [29, 30]

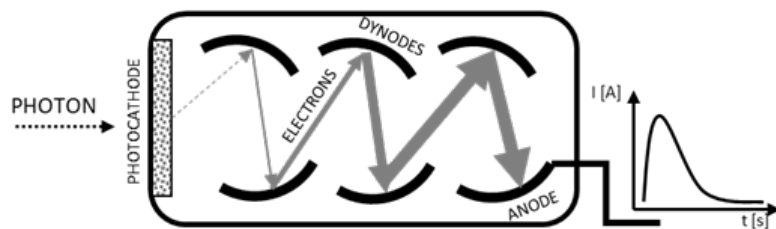


Figure 10: A PhotoMultiplier Tube

2.3 Preamplifiers

The internal gain of a PMT, obtained from the electron multiplication is sufficient for many applications. The produced current impulses can be detected with precise circuitry, however there are multiple reasons for which a preamplifier is often used in tangent with a PMT. With a typical load of 50Ω the output signal of a single photon is a very sharp voltage peak of around 10 mV. Unprocessed short PMT pulses are sufficient for detection, counting and timing, but may be problematic when it comes to discrimination and processes like Pulse Height Analysis (PHA). [31]

In those scenarios that do not require the sharpest response, the slight increase in Signal to Noise Ratio is worth the features introduced by an amplifier. These can include impedance matching, filtering and pulse-shaping. In tokamak applications it also helps move most of the diagnostic infrastructure away from the dangerous environment created by the fusion plasma.

Amplification is required in applications where the processing instruments cannot be connected directly to the detector. Long wiring is susceptible to electromagnetic interference, so the milivolt signal produced by a raw PMT would get drowned out in such scenarios.

2.4 Pulse processing chains

To obtain a radiation spectrum from the voltage pulses, their height must be measured and placed into an appropriate bin consisting of a range of voltage levels. The pulses generated by a PMT last just a few nanoseconds, making the task at hand complicated.

With a preamplifier this duration is increased by a factor of around a few hundreds depending on the preamplifier components. This results in pulses that last a few hundreds nanoseconds. Before the advent of ultra-high speed Analogue to Digital Converters (ADCs), such short events could not viably be processed with digital electronics and had to rely on analogue components.

2.4.1 Analogue processing chains

In analogue radiation spectroscopy pulses are typically first transformed to a Gaussian shape, with a series of low- and high-pass filters. These signals must then pass through complicated pile-up rejection circuitry. After that the pulses are fed to a Multi Channel Analyzer (MCA). This is the device that performs the binning action. Initially an MCA would consist of an array of analogue comparators, and over time it would rely on more and more digital components. The schematics of a typical analogue system are shown in Figure 11

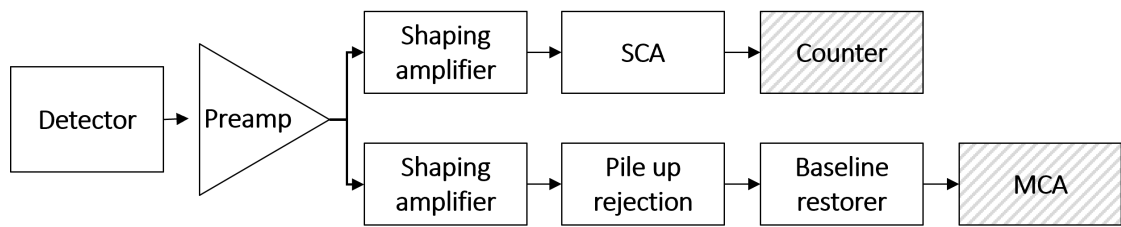


Figure 11: Analogue Pulse Processing chain

As mentioned earlier, for a long time analogue processing was the only way to reliably handle events shorter than 100 ns. It was, however, quickly recognized that the digital approach offered much lesser susceptibility to outside noise. Digital components could also potentially be tuned without having to physically modify the circuit. These two features are particularly important in the complicated environment of a fusion reactor. [32]

2.4.2 Digital processing chains

As soon as ADCs and digital processing circuits capable of reaching the resolution required for precise nuclear spectroscopy appeared on the market they were adopted into new experimental designs of MCAs [33]. As the technology improved ADCs were moved closer to the radiation detector itself. A single reprogrammable silicon chip, together with a fast ADC, could perform the job of a number of the analogue components in a spectroscopy system. On top of that its operation is less susceptible to Electro Magnetic Interference (EMI) and temperature-induced parameter variance. [34]

The earlier in a processing chain that the ADC is placed the lesser the influence of imperfect analogue components is. Seeing an ADC right after the preamplifier is commonplace in modern systems as shown in Figure 12. Such approach, however, produces an

important issue. To obtain a sufficient horizontal resolution comparable to analogue chains the ADC must sample the signal with a frequency of at least a few hundred MHz. This means that, at a typical vertical resolution of anywhere between 8 to 16 bits, a modern high-speed ADC can generate anywhere between 100 megabytes up to even a few gigabytes of data every second. [34]

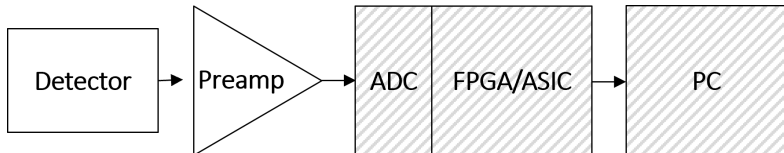


Figure 12: Digital Pulse Processing chain

Processing gigabytes of data in real time poses one of the primary challenges in designing Digital Pulse Processing systems. Despite that, fast digitizers are used for Hard X-Ray Spectroscopy in existing tokamaks, like KSTAR or JET [28, 35]. ITER will require similar or better systems during its operation, so the problems of handling large data throughput should be considered solved before the diagnostic systems are installed in the facility. Once first plasma is obtained, the possibility of system modifications will be greatly limited.

2.5 ITER HXRM specification

The Hard X Ray Monitor planned to be installed at ITER will have to meet very specific requirements. The device has to operate in two modes. The first standard mode is the pulse counting mode. In it the pulses produced by the PMT have to be detected, categorized and binned. This actions has to be performed continuously over a configurable time period between 1 ms and 10 ms. Each sampling window must then produce an energy spectrum of the collected pulses. [36]

Although storing the entire spectrum is useful for research purposes, two figures must be transferred as quickly as possible to the Plasma Control System (PCS), so that critical decisions regarding the tokamak's safety can be made. The PCS requires the maximum runaway electron energy measured and the total count to operate. This data has to be made available with a latency lesser than 5 ms after each 10 ms sampling window finishes. [36]

When the number of runaway electrons becomes overwhelming for the PMT detector, the signal produced by the device will appear closer to a constant current, due to the

pulse overlap. When that scenario occurs the HXRM must switch into its second mode of operation, the current mode. In this mode PCS must be made aware of the current magnitude measured over the same time window. It is expected that a switch to current mode must be made when the number of pulses exceeds 10^6 counts per second.

On top of the spectral information sent to PCS, the device should also transfer raw samples with the detected pulses to a Data Archiving Network (DAN) for offline analysis and diagnostics. Table 1 lists the most important parameters that ITER's HXRM must meet. The table includes parameters related to operation in both counting and current modes.

Table 1: Selected ITER's requirements for the HXRM [36]

Parameter	Value
<i>RE Energy Range</i>	0.1 MeV to 100 MeV
<i>Required energy resolution</i>	20%
<i>RE current to be detected</i>	10kA to 15 MA
<i>ADC sampling period</i>	2ns
<i>Number of ADC channels</i>	2
<i>Max. detector temperature</i>	$240^\circ\text{C} \pm 10^\circ\text{C}$
<i>Max. magnetic field</i>	5 T

To meet the requirements regarding temperature and magnetic field, as well as the space constraints, some important considerations were taken. In ITER the X-Ray radiation will first be converted to a light pulse. Only the scintillator will be exposed directly on the front wall. The PMT detector will be connected to the scintillator via a 12 m long optical fiber. The PMT will then interface to the processing system via a 100 m long coaxial cable. [37]

The attenuation of fiber optic is usually specified in dB/km so 12 m is a length insufficient to generate meaningful light loss. The critical issue lies in the connectors. Mis-coupling of fiber optic connectors can generate a massive signal loss. In a tokamak's environment it will be nearly impossible to keep the connectors perfectly aligned due to vibrations, temperature variation and magnetic fields. It is thus likely that just a few promilles of the photons generated by the scintillator will actually reach the PMT. [37]

3 Research setup

An FPGA powered data acquisition board was used as the platform for the hardware implementation of digital pulse processing of PMT signals. The following subsections describe the system component in detail and Figure 13 shows an overview of the test bench. A 25 kBq ^{137}Cs radioactive sample was placed in a plastic V-vial and used to test the setup.

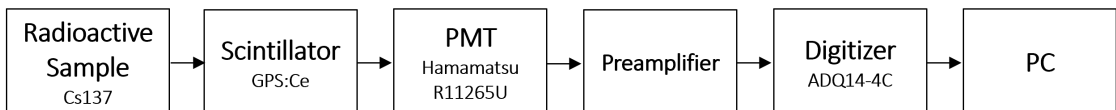


Figure 13: HXRM test bench overview

3.1 PMT

Hamamatsu R11265U served as the PhotoMultiplier Tube. A 15 mm GPS:Ce scintillator wrapped in aluminium foil was connected coupled directly to the PMT to generate light pulses from the radiation. The PMT with the scintillator and radioactive material were placed in a dark container and held together with a custom-designed 3D printed casing.

3.2 Preamplifier

The design of a preamplifier capable of transforming the PMT output signal is a non-trivial task. Nearly no commercially available amplifiers offer parameters that satisfy all of the requirements. Specifically for this project, a custom low-noise preamplifier has been developed by Nowakowski et al. and described in another paper. The PMT-Preamplifier combination generated pulses that could be fit to a single exponential model with a decay constant of 130 ns. [25]

3.3 Digitizer board

To acquire and digitize the signals produced by the PMT and preamplifier combination Teledyne SP Devices ADQ14-4C was used. The board was connected through PCIe 2.0

to the host PC running custom acquisition software. ADQ14-4C can sample signals from up to 4 channels, each at a maximum frequency of 1 GHz.

Table 2: Chosen parameters of ADQ14-4C

Parameter	Value
<i>Channel count</i>	4
<i>Sampling rate</i>	1 GS/S
<i>Vertical resolution</i>	14 bits
<i>Interface</i>	PCIe 2.0 x8
<i>Max. data transfer rate</i>	3.2 GB/s
<i>Internal DRAM memory</i>	2 GB
<i>Input range peak to peak</i>	0.2 V - 10 V
<i>Number of GPIO ports</i>	12

The ADQ14 acquires samples with a 14-bit ADC. The device applies factory calibrated digital gain and shift to the raw measurements, so in order to maintain higher precision the samples are extended to 16 bits representing two full bytes. The additional two bits represent the fractional part potentially produced by the fractional gain component.

The ADQ14 can operate in both triggered streaming and continuous mode. In continuous mode samples are constantly gathered and periodically transferred to the host PC. In triggered streaming a window of samples is collected only after a trigger event is detected. This is a basic feature that allows for some data reduction, as only events of interest have to be transferred to the host PC. Multiple triggering mechanisms, like level, periodic and external are available.

In all modes of operation the device relies on an internal 2 GB DRAM to act as a FIFO queue for the generated records. The device relies on Direct Memory Access (DMA) to transfer data to the host PC. This is a special mode of operation for peripheral devices in which a chunk of the computer's memory is made available to them without the need of CPU brokerage.

Unfortunately the maximum size of DMA buffers is limited. With a sampling speed of a 1 GHz and 2 byte samples up to two gigabytes of data can be generated each second for each channel that is active. Even with reliance on DMA maintaining a transfer speed this high is problematic. To solve this issue, the ADQ14's internal DRAM acts as a buffer whenever the throughput becomes too high. Records are first stored in the internal DRAM and periodically transferred to the host PC's RAM whenever buffers become ready. At maximum speed a single channel can, however, still fill the entirety of this

buffer in just a second if its contents are not processed in time.

3.3.1 Open FPGA design

A crucial feature of ADQ14 is the fact that its core processing functionality is realised with the use of an on-board FPGA, more specifically a Xilinx Kintex 7 K325T. The design of the FPGA is partially open. Users can implement custom filtering or data analysis on samples in real time. This fact is used to implement the custom pulse processing described in this work.

The firmware is unfortunately not entirely open-source. Third-party IP cores cannot be distributed to end customers and thus user algorithms are limited to two sections called User Logics. User Logic 1 is a core placed after the ADC samples are subjected to factory gain, but before the signals are passed on to trigger control. This enables the implementation of custom triggering logic.

User Logic 2 is intended to house more complicated logic. This module has access to the GPIO ports and some metadata outputs, that can be used to better describe the transferred records. User Logic 2 is located right before the encrypted packet generator that is responsible for queueing the incoming data in ADQ14's DRAM for transfer to the host PC. The packet generator can be partially controlled from within User Logic 2. Arbitrary data can be injected in place of the samples for each channel and the size of transferred windows can be modified.

3.3.2 Parallel sampling

The FPGA is clocked only at 250 MHz which is exactly a quarter of the ADC maximum operating frequency. This means that each channel of the digitizer outputs 4 samples on each clock cycle of the FPGA. This is a necessary design choice as FPGAs fare better at lower clock speeds due to the need of less complex routing when it comes to connecting the various peripherals and CLBs.

Such design does however complicate the implementation of Digital Signal Processing. It is especially cumbersome for functions that depend on delayed samples. Accumulators have the need of summing up 4 samples on each clock cycle instead of one. Complicated operations like multiplication and division require duplicated logic. Most functionality must be properly pipelined to avoid timing issues in the FPGA design.

3.4 Host computer

The host computer was running Red Hat Enterprise Linux 7. Table 3 lists the computer hardware configuration.

Table 3: Hardware configuration of the host PC

Parameter	Value
CPU	Intel Xeon C5549
Storage	Samsung 970 EVO Plus 500 GB
Operating System	Red Hat Enterprise Linux 7.4
GPU	NVIDIA GP107
RAM	24 GB DDR3 1333 MHz

3.5 Software package

To control the acquisition process and handle the data transfer, a custom software GUI application was developed. The application employs an API provided by SP Devices to interface to the digitizer board. The Qt5 framework is used for GUI display and multiple other functions. The application leverages the Qt's signal/slot system heavily to synchronize threaded events.

The primary thread of the software application is used for UI display and general tasks like loading and saving configurations. A secondary thread is spawned to control data acquisition and archival. The proper operation of the secondary worker thread is crucial in obtaining a high data throughput and the process of software optimization is described in section 7

4 Pulse detection

In order to process any pulses they must be first detected. The window of interest containing a pulse to be analysed must be properly distinguished from the surrounding noise. Although detection is a must, it also brings the added benefit of data rate reduction. If pulses can be accurately marked within a signal it is possible to transfer only those samples that compose the events to the host PC.

The ADQ14 is capable of sampling signals with a frequency of up to 1 GHz. With two bytes per sample, a single channel generates 2 GBs of raw data per second. For the PCIe 2.0 interface, that is used in this work, the manufacturer's datasheet specifies a theoretical maximum throughput of 3.2 GB/s. Even if this perfect limit could be obtained it would not allow for two channels to be active at once. Using pulse detection for data reduction is thus unavoidable. It is crucial to use a robust algorithm for this process to ensure that almost no pulses go unnoticed and near to none false positives are transmitted.

4.1 Level trigger

The most basic approach to detection is a level trigger, a technology available in virtually any spectrometer. As shown in Figure 14, a trigger occurs when the input signal crosses a predefined voltage level, either on a rising or a falling edge. The point at which this happens marks the beginning of a record window. In the simplest case the end of a window is placed a fixed duration from the start. Samples within that window form a region of interest and are transferred further down the processing pipeline.

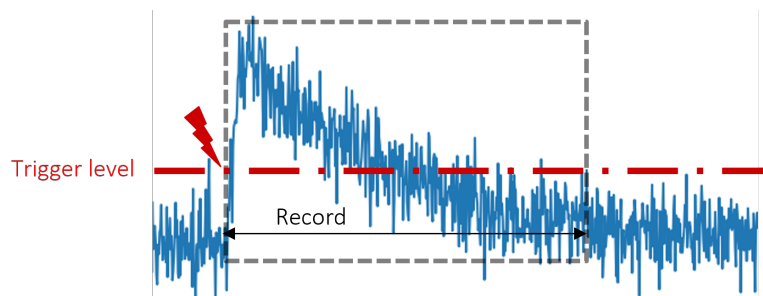


Figure 14: Level trigger

Once a window finishes, no more events are detected until the signal returns to a value below the trigger level (for rising edge triggering). This reset value might be set to be

equal to the trigger level, however such approach might lead to a scenario shown in Figure 15. In a noisy environment the signal might falsely trigger immediately after a window ends due to a random high spike on the slower falling edge of an exponential pulse.

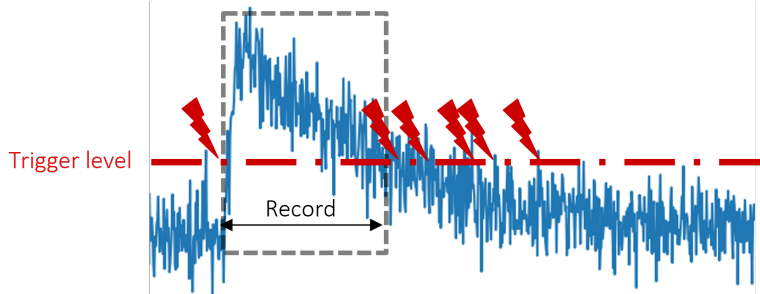


Figure 15: Level trigger with no hysteresis

To prevent such false triggers typically some form of a hysteresis is used. The reset level is shifted downwards, so that the input signal must cross such a threshold that the random noise is almost guaranteed to never cause false triggers. Figure 16 shows a hysteresis mitigating some false triggers. Some of the false triggers from Figure 15 are removed, however due to the high noise some still persist.

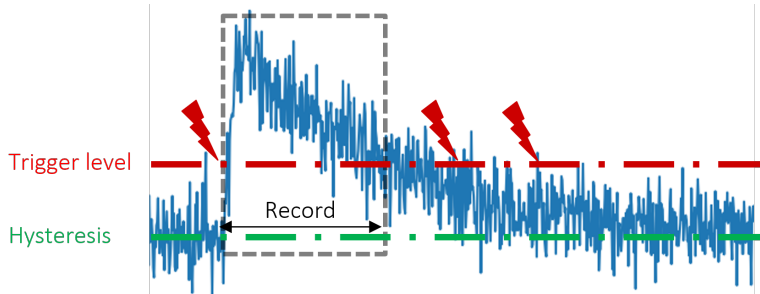


Figure 16: Level trigger with a hysteresis

With the slow falling edge of a pulse care must be taken not to overestimate the hysteresis. By setting the reset level too far away from the trigger level pile-ups can be missed as pointed to in Figure 17. With a properly set hysteresis the level trigger offers performance that is sufficient in most applications, as suggested by its prevalence in modern spectrometers. In a tokamak's environment, however, the hysteresis alone could potentially prove insufficient due to electromagnetic and temperature fluctuations having an effect on noise.

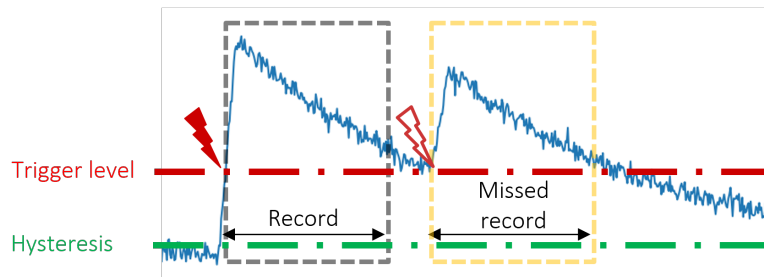


Figure 17: Level trigger hysteresis causing missed events

4.2 Boxcar filter

The two problems most apparent to simple level triggering are its susceptibility to noise and pulse overlap. Just as with analogue approaches these two problems can be minimized with low-pass and high-pass filtering. By utilizing a low-pass filter the input signal becomes smoother and more averaged, reducing the possibility of false triggers caused by random spikes. A high-pass filter would reduce the DC component of the falling edge of a pulse, making pile-ups easier to detect.

In the digital domain the simplest filters that perform these operations are the Moving Average (MA) filter and the derivative filter. MA works to reduce the spikes and increase SNR. The derivative filter can strip the DC component from a signal, meaning that the sharp rising edges will become more attenuated in comparison to the decaying tails.

By combining the concepts of the MA and derivative filters into a single a Boxcar filter is obtained. Figure 18 shows an example Boxcar transfer function, together with its effect on an input signal of two exponential pulses. The boxcar filter can be considered to be a subtraction of two samples averaged with a window of length W delayed from each other by W . On Figure 18 $W = 25$.

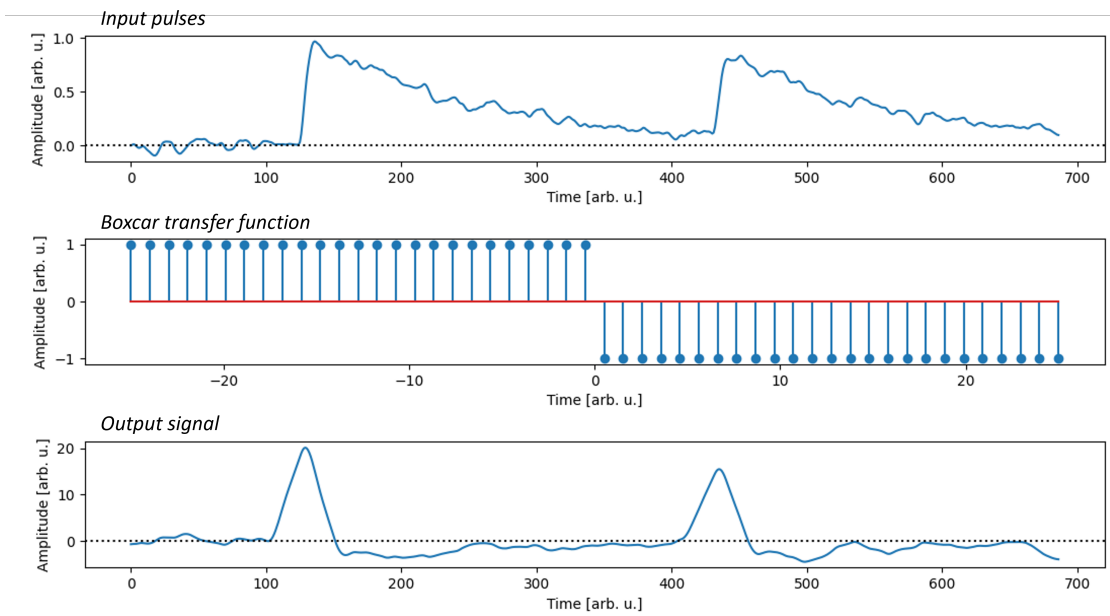


Figure 18: Effect of boxcar filtering on two exponential pulses

With basic level triggering on the raw pulses the trigger position will be the later in a pulse the shorter it is. Pulses that reach just slightly above the trigger level will be detected near their top, while pulses significantly stronger than the trigger level will be detected near their start as shown in Figure 19. This behaviour is called amplitude walk.

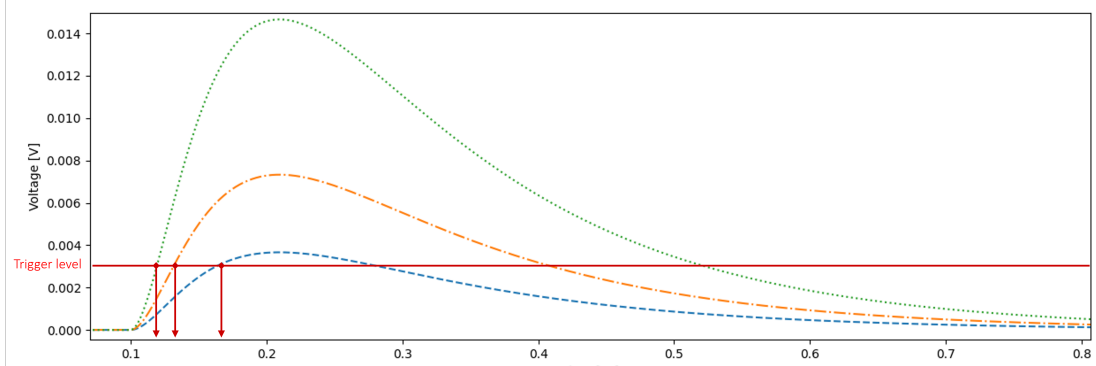


Figure 19: Amplitude walk

The derivative part of the Boxcar filter can be used in a digital Constant Fraction Discriminator (CFD). The point at which a pulse's derivative crosses zero after the sharp rise marks the peak of the original pulse. When using averaging from the boxcar filter this position will be slightly shifted but can still be reliably used to increase the timestamping precision.

4.3 Trapezoidal filter

The trapezoidal filter shapes incoming pulses into the shape of an isosceles trapezoid. The sharp rising edge and slow decay tail are replaced with same length mirrored edges. Instead of a sharp peak a flattop region is formed that is proportional to the pulse height. The length of edges and the flattop can be freely controlled through constants in the filter. Figure 20 shows the effect of a trapezoidal filter being applied to a train of two exponential pulses. Note the dotted trigger line almost causing a false negative if applied to raw signal. The filtered signal provides a clear distinction between the slightly overlapping pulses.

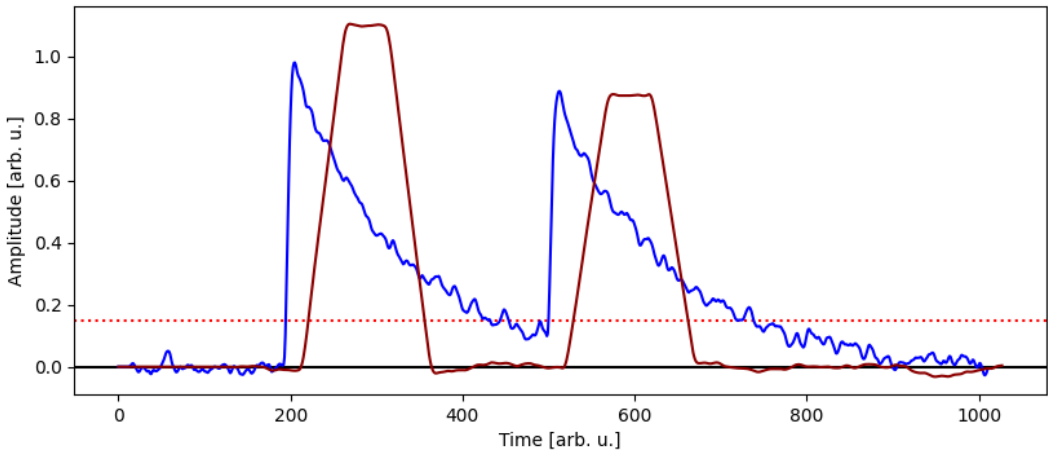


Figure 20: Trapezoid filter applied to a train of two pulses

The trapezoidal filter is a more complicated filter than the boxcar filter. It relies on the use of a Moving Window Deconvolution (MWD), as first proposed by Georgiev et al. [38]. It is trivial to obtain a trapezoidal shape from a step input function. The MWD algorithm works to transform an exponentially decaying pulse into a step signal. A step function, while perfect for transformations, is undesirable in continuous mode of operation. With multiple pulses, they form a staircase and eventually saturate. The simple solution is to perform a subtraction of a delayed sample. This changes the step signal to a rectangular shape with a length defined by the delay amount. The staircase then becomes a train of rectangular pulses. Figure 21 shows the consecutive steps of a MWD algorithm.

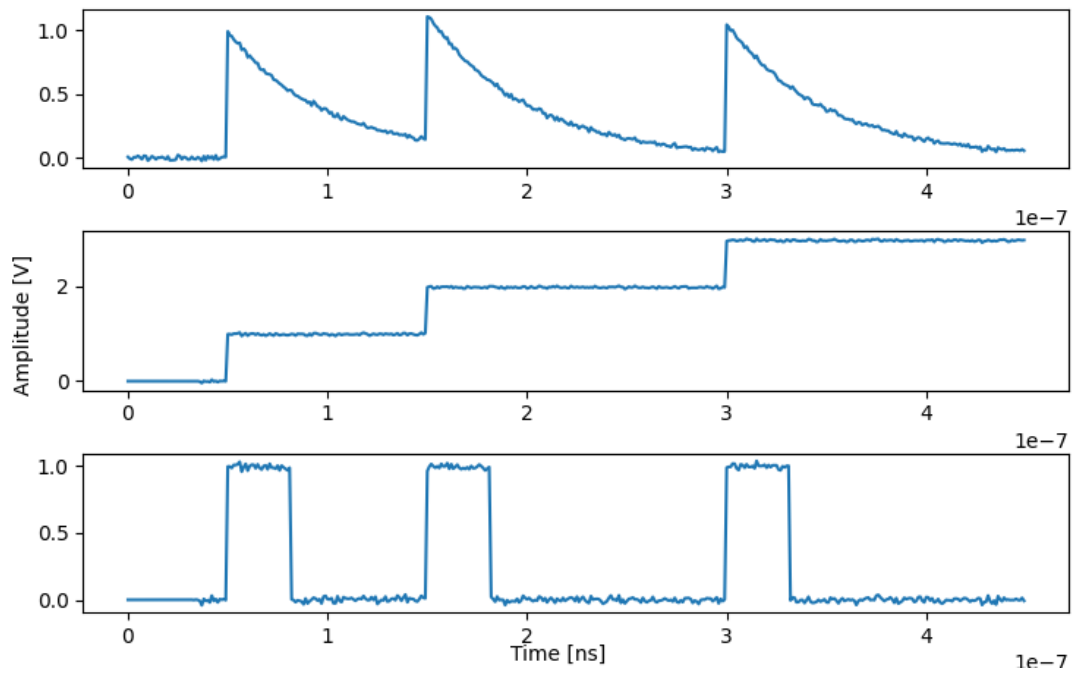


Figure 21: MWD algorithm applied to a series of 3 pulses

MWD requires the precise value of the pulse decay constant to be known. Figure 22 shows the effect of using a wrong value when configuring the MWD filter. By tuning the filter with a time constant that is too high an undershoot is obtained after the rectangular shape. Using a value that is too low causes and overshoot. Both mistakes reduce the accuracy of pile-up discrimination, as consecutive pulses will overlap with the decaying region.

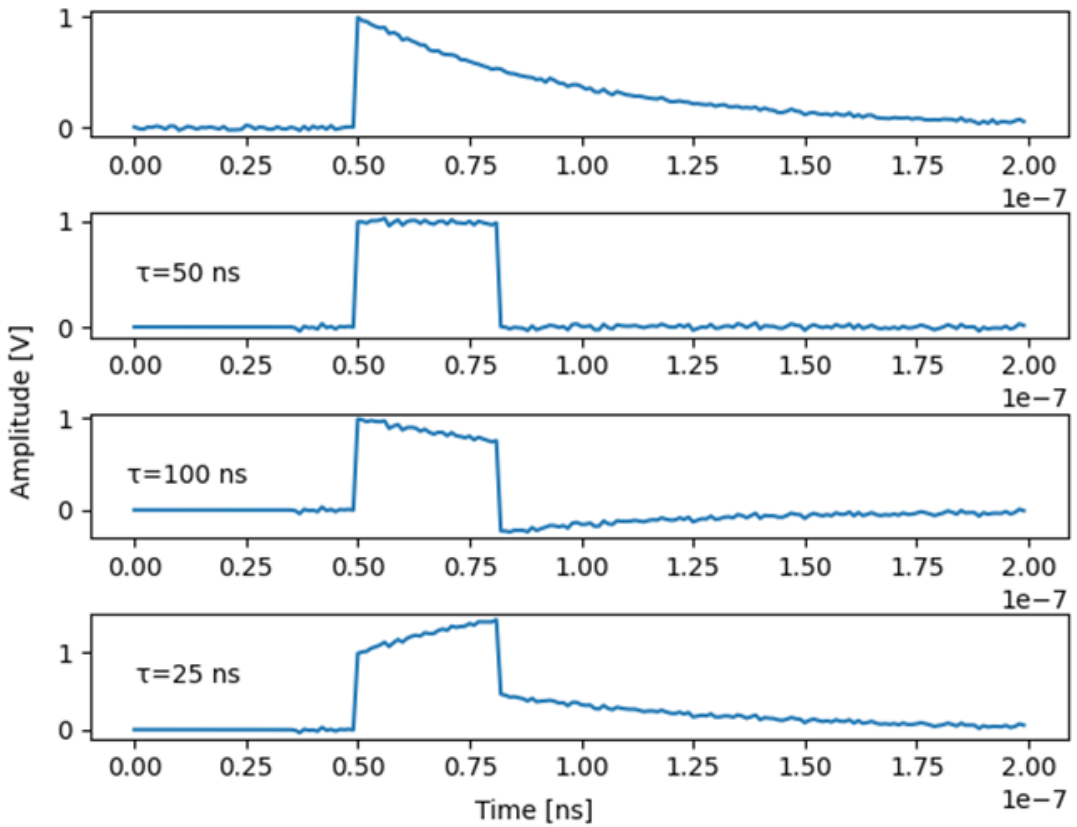


Figure 22: The effects of decay constant mismatch between a pulse and a MWD algorithm. Decay constant of pulses is 50 ns.

The MWD algorithm itself produces a rectangular shape. To obtain a trapezoid an averaging step is applied. This causes the edges to smoothen and as a side effect decrease the noise as shown in Figure 23. The trapezoid filter can also be synthesized using alternative methods that are better optimized for hardware implementation. MWD itself requires division which is an extremely resource consuming operation in digital signal processing.

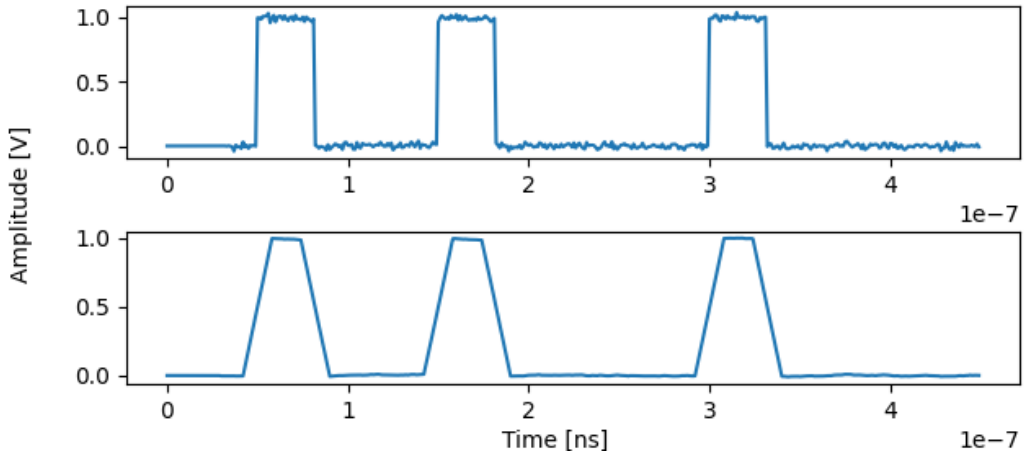


Figure 23: Last step of synthesizing a trapezoid with the use of MWD

4.4 Triangular filter

As mentioned earlier the flattop region of a trapezoidal filter is not particularly useful for pulse detection. By using an averaging filter with the same window length as the MWD window, the flattop is squeezed and a triangular shape is formed as shown Figure 24. Thus, the triangular filter is a special case of the trapezoidal filter that can be used if only detection or timing is of interest.

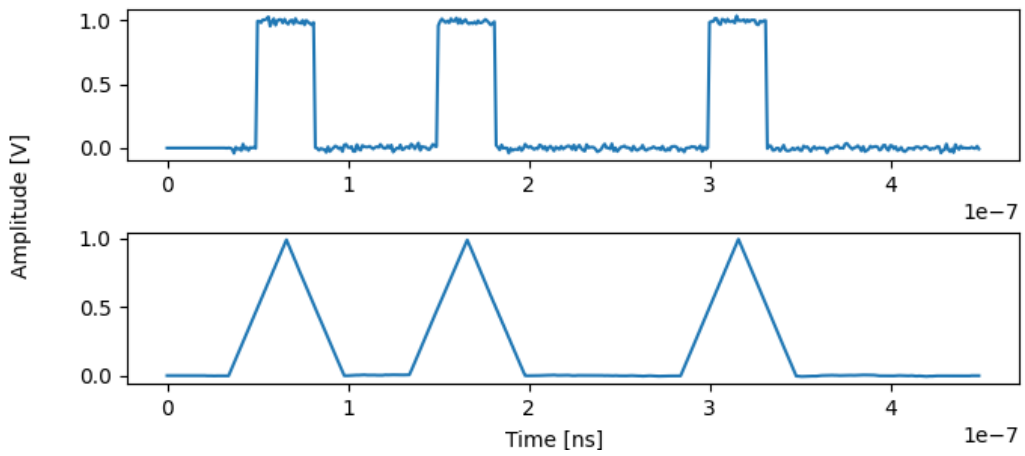


Figure 24: Triangular filter being formed as the last step of a MWD

4.5 Other pulse detection methods

Other methods and filters for detection apart from those described above can be found in scientific literature. They have not been chosen for implementation in this work due to their low maturity, excessive complexity or subpar performance. Low hardware resource usage and minimal delay were some of the primary parameters considered due to the need of real-time processing of incoming pulses.

Faisal et al. used normalized cross-correlation to compare the similarity of incoming pulses to a predefined ideal template pulse. The algorithm was implemented in an FPGA at a sampling rate of 250 MS/s. When compared to amplitude thresholding, their method improved the probability of correct pulse detection by a factor of 4 when a template obtained from averaging capture pulses was used; and by a factor of 3 when a greatly simplified square model was used. [39]

Kamleitner et al analysed and compared a multitude of different edge detection algorithms. Apart from algorithms similar to the trapezoidal filter and the boxcar filter described above, the work analyzed three similarity matching algorithms, Canny's edge detector, as well as optimally designed FIR filters. The optimum filters won the benchmarks, however, they were closely followed by the boxcar-like Single Delay Line as well as the trapezoidal filter. Similarity filters fared significantly worse, offering superior performance only when it came to the number of false positives. [40]

4.6 Simulation performance

In order to find the most suitable filters for hardware implementation in the Hard X-Ray Monitor the algorithms were first subjected to a series of simulated software tests. Level triggering, zero crossing detection, triangular and boxcar filtering were implemented with the use of the numpy and scipy libraries in Python. The same libraries were used to create a test bench for generating simulated impulses with a configurable frequency, noise, amplitude and decay constant.

The test pulse trains were fed to the filters and each output was tested with an array of different trigger configurations. The trigger level and reset at which the cost function was lowest for a given algorithm was chosen as the representative record for comparison between different filters. For each record the number of properly detected pulses (true positives), missed pulses (false negatives) and noise mistaken for pulses (false positives) were counted and divided by the total pulse count. This is crucial, as the

pulse count was higher in tests that checked behavior under high pile-up conditions.

For initial filter functionality tests and debugging, a graphical user interface was prepared with the use of the matplotlib library. The tool would run a test scenario, generate a train of pulses with the specified parameters, filter the input signal and run user-configured level triggering on the output signal. The end result would be a plot superimposing the input and output signals. Detected pulse were marked with a green rectangle. Missed pulses showed up as red dashed rectangles and wrongly classified noise was marked with an orange color. Figure 25 shows an example output from the graphical tool. A boxcar filter is used to improve the performance of detection. In the example one pulse is not detected due to pile-up and one is not detected due to a badly configured trigger threshold.

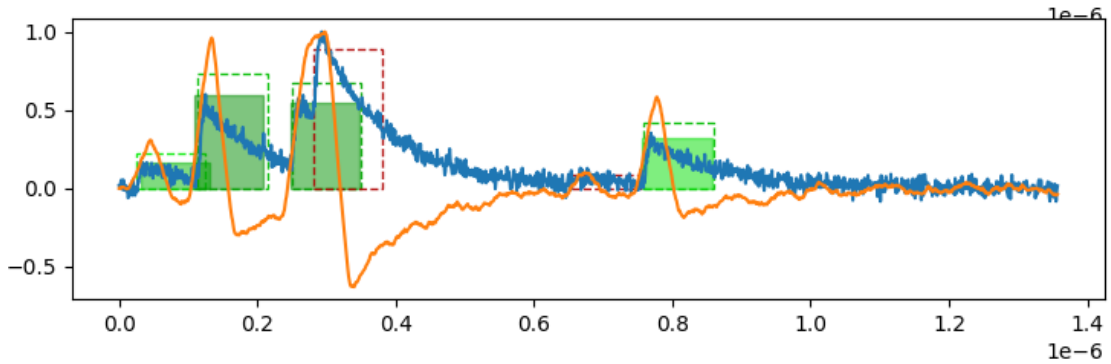


Figure 25: Example output from the graphical tool for debugging detection filters

Once the filters and the testbench were rid of bugs and optimized with the graphical tool, it was modified for automated testing. Instead of using user-specified trigger levels the script would test a range of settings to find the best ones. In place of the graphical result a confusion matrix for each approach was used. The best results from each algorithm were then plotted on one graph to obtain a figure of merit based comparison for different methods.

?? and ?? show the results of the simulations. The cost function used to rate the filters was a sum of false negatives and false positives divided by the total number of pulses that actually were present in the simulation. Both triangular and boxcar filters provide an immense improvement over level triggering on raw signal. A triangular filter with the same max delay length provides slightly better accuracy than a boxcar filter.

While a filter with a longer averaging effect (longer window length) fares better in noisier environments, as indicated in figure Figure 27, the inverse is true when it comes to pile-

up frequency. Shorter filters have a higher likelihood of discriminating between two overlapping pulses as shown by the results in Figure 26. There is no detection filter that is best for all applications. The filter must be tuned to a specific use case, however some filters, like the Boxcar offer a simpler interface for doing so, than others.

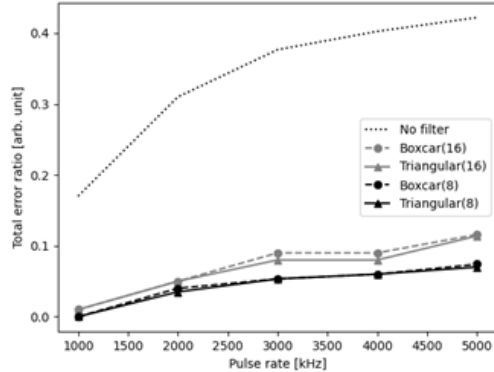


Figure 26: Detection algorithms compared under varying pulse frequency

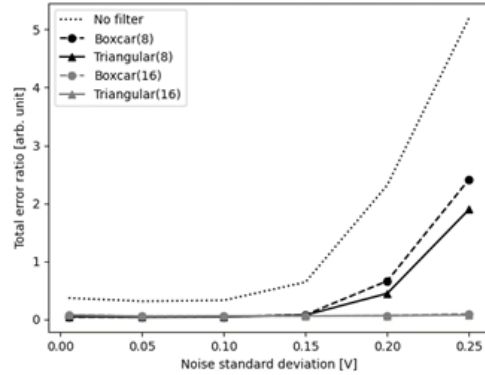


Figure 27: Detection algorithms compared under varying noise magnitude

5 Pulse Height Analysis

The amplitude of a pulse generated by a PhotoMultiplier Tube is directly proportional to the energy carried by a Runaway Electron. By measuring the height of the signal peak it is thus possible to estimate the RE energy and produce an X-Ray radiation spectrum. The previous chapter described methods that can be used for the detection of such pulses. This section focuses on methods that can be used on top of the detection algorithms to obtain the best possible resolution of the pulse height measurement.

5.1 Pulse shaping algorithms

As described in subsection 4.2 the zero crossing point of a pulse derivative pinpoints its peak. The simplest method of obtaining the pulse height is thus using a derivative and sampling the original signal at the zero-crossing. The method works, however it is highly susceptible to noise. Taking only a single sample grants a result with a precision equal to the noise magnitude. It would be beneficial to take multiple samples of the signal height, to minimize the error.

Pulse shaping algorithms help reduce the influence of noise on the peak height measurement. Analogue pulse processing systems typically relied on CR-RC filters to shape pulses to a more Gaussian shape. This granted them a smoother peak that could be averaged over multiple samples. In the digital domain a trapezoidal filter (see ??) is the most commonly chosen shaping filter.

When used for pulse detection, the flattop region of a trapezoid-shaped pulse is of little interest, and can be truncated to form a triangular filter. In Pulse Height Analysis, the near constant signal produced by the trapezoid is a crucial feature. Instead of taking a single sample at the sharp peak, multiple samples are taken throughout the whole flattop region. Longer flattop region provides better noise immunity but the it has an upper limit dictated by the pile-up frequency.

5.2 Integration

The pulses generated by a PMT-preamplifier combination have a constant decay time and differ in amplitude. They can be fairly accurately modelled with a single exponential formula: Ae^{-t} , where A is the pulse amplitude, and t expresses time, assuming that the

pulse peak occurs at $t = 0$. The surface area under the curve given by that formula is proportional to the amplitude A .

The pulses can be integrated to obtain a value that is proportional to the pulse amplitude and RE energy. As multiple samples over the pulse duration are accumulated the effect of noise is minimized just like with trapezoidal shaping. Integration is a simpler procedure to implement than shaping and timing filters. It does not require the precise decay time to be known. This is beneficial as a single-exponential function is only an approximation of a preamplified signal.

While integration only requires the use of a single accumulator to add the samples up, it results in a numerically large final sum. To obtain a usable result this value must be scaled down to a usable range. For example a range corresponding with the ADC codes is a good choice. An integral of a pulse is then mapped to value equal to its amplitude. This constant divider can be calculated for a fixed sampling window length or obtained experimentally.

The biggest drawback of using integration is its susceptibility to pile-up effects. To obtain accurate results in environments with high pile-up or long pulse decay, complicated pile-up compensation must be used. These algorithms work to subtract or otherwise remove already detected pulses from the input signal. Although such solutions have been proposed in research work, their implementation is expensive and usually limited to a single pile-up of just two pulses. [41]

5.3 Simulated performance

6 HXRM firmware

Based on the results of research and simulations, the best timing and shaping algorithms were implemented in hardware. The ADQ14 uses Verilog and Vivado 2015.2, so these tools were chosen for the implementation of the HXRM. The developed system performs pulse detection, measures the peak height, stores the resultant spectrum and periodically transfer the results to the host PC.

6.1 System overview

As described in subsubsection 3.3.1 the ADQ14 DevKit grants a semi-open FPGA design with two modules that can be freely modified by the end user. The board manufacturer designed User Logic 1 with intent for it to house timing filters and User Logic 2 to contain more specialized processing logic. Initially, these ideas were followed with a Boxcar filter being implemented in User Logic 1 and a Pulse Height Analyzer being placed in User Logic 2.

With the default firmware, ADQ14 generates fixed-length records on trigger events. For example, with the window length set to a 1000 samples, upon the detection of a pulse, 1000 samples would always be transferred to the PC, regardless of pile ups and other disturbances. For this reason the timing logic originally placed in User Logic 1 was moved to User Logic 2, so that it could be better integrated with the rest of the pulse analysis systems. The UL2 module allows for full control over record lengths so sampling windows in which pile ups were detected could now be rejected, split into two or prolonged depending on the need. Figure 28 gives an overview of the system designed in User Logic 2.

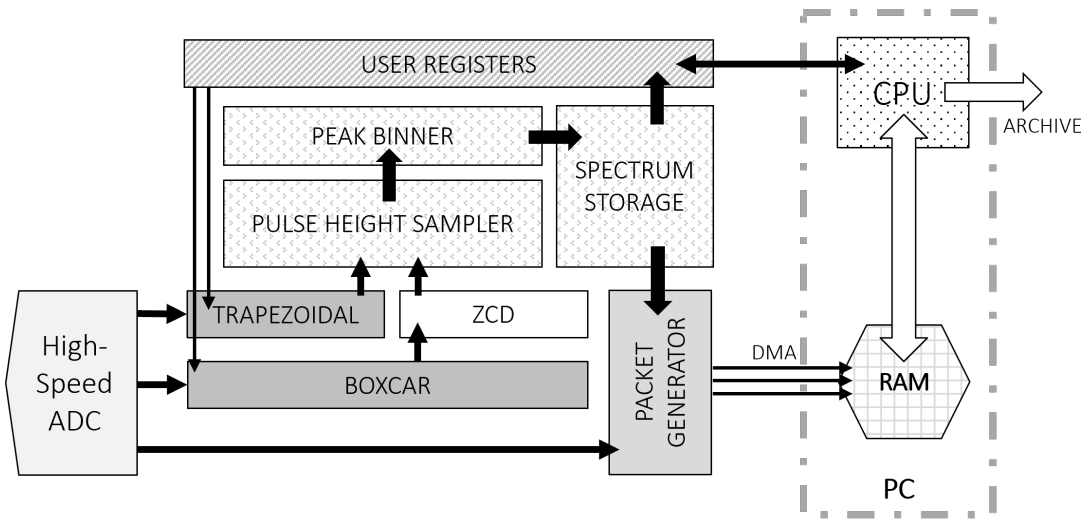


Figure 28: Firmware overview in User Logic 2

6.2 System control

The system is configured and controlled through so called user registers. 2^{19} individually addressable 32-bit words are available for reading and writing to from the PC. The first four words are reserved for internal use. Next four have been dedicated for configuration and control as listed in ???. The 2^{14} block of addresses starting from position 9, can be used to read values from bins forming the currently held spectrum.

6.3 Pulse detection

Pulse detection relies on the use of a configurable boxcar filter that then passes through a zero crossing detector. Depending on the length of the boxcar window the result of the ZCD is delayed by an appropriate amount so that it points to a point at which the trapezoidal filter's rising edge starts. To prevent false triggers the ZCD operates in two modes. First it awaits a user specified threshold value to be crossed. Only after that event occurs, does it start looking for a zero crossing. After a zero crossing the system returns back to the threshold awaiting state. Figure 29 illustrates this algorithm. The threshold value is transferred through user registers and does not require the FPGA to be reprogrammed if modified.



Figure 29: Zero Crossing Detection algorithm employed in firmware for pulse detection and timing

The implementation of a boxcar filter in firmware required a few considerations due to the parallel sampling described in subsubsection 3.3.2. The general formula for a boxcar filter can be described as follows:

$$y(n) = \frac{1}{W} \sum_{i=n-W+1}^n x(i) - \sum_{i=n-2W+1}^{n-W} x(i)$$

W stands for the boxcar window length and $x(n)$ is the input signal. The mathematical formula requires the use of two moving average filters. The pseudocode below describes the Register Transfer Level behaviour used to implement an optimized Moving Average filter in firmware.

```

for parsamp in [3...0]:
    ma_0[parsamp] <= x[parsamp] - x[parsamp+W];
    ma_1[3] <= ma_0[3];
    ma_1[2] <= ma_0[3] + ma_0[2];
    ma_1[1] <= ma_0[1];
    ma_1[0] <= ma_0[1] + ma_0[0];
    ma_2[3] <= ma_1[3];
    ma_2[2] <= ma_1[2];
    ma_2[1] <= ma_1[2] + ma_1[1];
    ma_2[0] <= ma_1[2] + ma_1[0];
    for parsamp in [3...0]:
        ma_3[parsamp] <= ma_3[0] + ma_2[parsamp];
        divided[parsamp] <= ma_3[parsamp] / W;
        y[parsamp] <= divided[parsamp] - divided[parsamp+W];

```

Four parallel samples are available on each clock cycle. To obtain an average they all must be added together. This requires the design to use pipelining. Attempting to add up 4 16-bit integers would violate the timing constraints specified by the FPGA. In other words, the synthesis tool could not route such a path in the device that this operation

would reliably execute at the 250 MHz clock frequency. Instead an optimized pipeline is used.

In the first step for each parallel sample a moving average is calculated as if the given sample was the only sample generated on each clock cycle. One sample outside now outside the MA window is subtracted and a new sample is added to the current rolling sum. In the next pipeline steps the four parallel samples must be added together. The proposed algorithm relies solely on two operand addition and requires one less clock cycle when compared to a simple cascading addition.

As the penultimate step the division over the window length is made. This is a very costly operation in terms of hardware usage. It can however be avoided if the possible window lengths are limited to natural powers of 2. In such case a division is equivalent to a right bitshift by a number equal to the power exponent. An integer divider would require around 20 clock cycles to complete. A bitshift can be very efficiently performed within a single clock cycle. Finally, to obtain the Boxcar, the divided values are delayed by the window length and subtracted. Figure 30 shows the optimized accumulator being realized with DSP blocks.

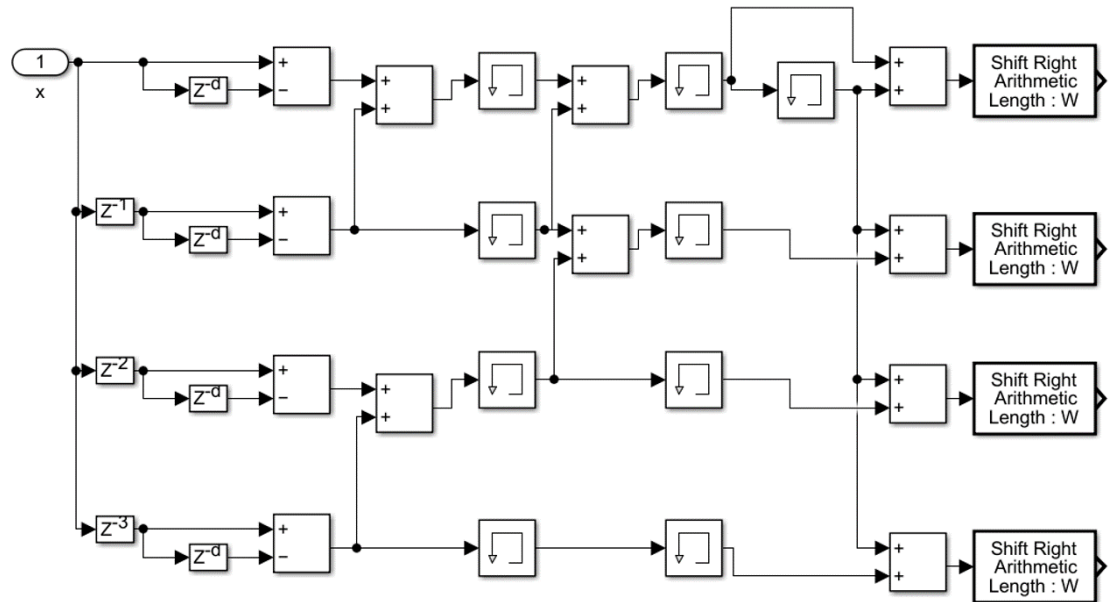


Figure 30: Timing optimized accumulator

6.4 Pulse height analysis

The timing generated by the ZCD is resynchronized to a trapezoidal filter, to indicate the start of a trapezoid forming. After a delay equal to the trapezoid edge the sampling module is triggered. The module accumulates every sample from the trapezoid flattop and divides the end result by the number of samples. The result grants an average flattop height that corresponds to the pulse peak height. The averaging action reduces overall noise and increases precision of the measurement. Figure 31 visualizes the algorithm.

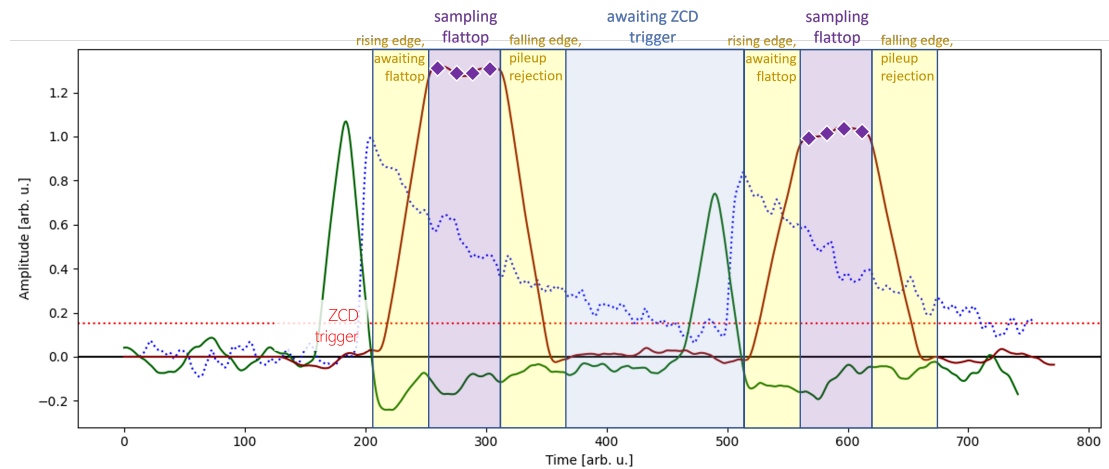


Figure 31: Trapezoid filter being used for pulse height analysis

Instead of the complicated MWD algorithm, a hardware-optimized design of the trapezoidal filter, described by Jordanov [42] is used. Figure 32 shows the filter being implemented with the use of DSP blocks. The design requires two accumulators, four addition blocks and one multiplier. Constant multiplication can be achieved with designs based on Look Up Tables (LUTs). If the operand M is a power of 2, the operation can be replaced with a left bit shift.

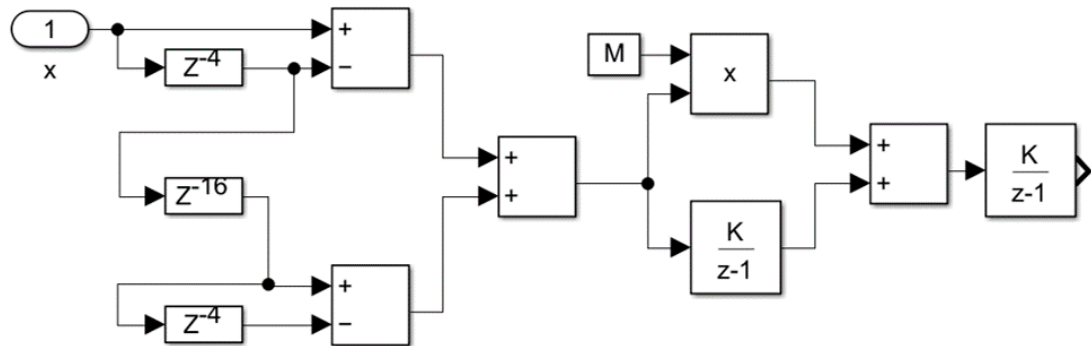


Figure 32: Trapezoid filter realized with the use of DSP blocks

The PHA firmware was programmed onto ADQ14 and run in parallel with an acquisition process. The firmware solution performed real-time spectroscopy. At the same time the raw signal was transferred to the PC. After an hour long acquisition finished, the raw signal was processed with a software algorithm and compared with the spectrum downloaded from the FPGA. Figure 33 shows the results of the real-time firmware spectroscopy overlaid with the offline processing method. The most important features of the ^{137}Cs sample are preserved in the hardware spectrum, suggesting a successful implementation of the described algorithm.

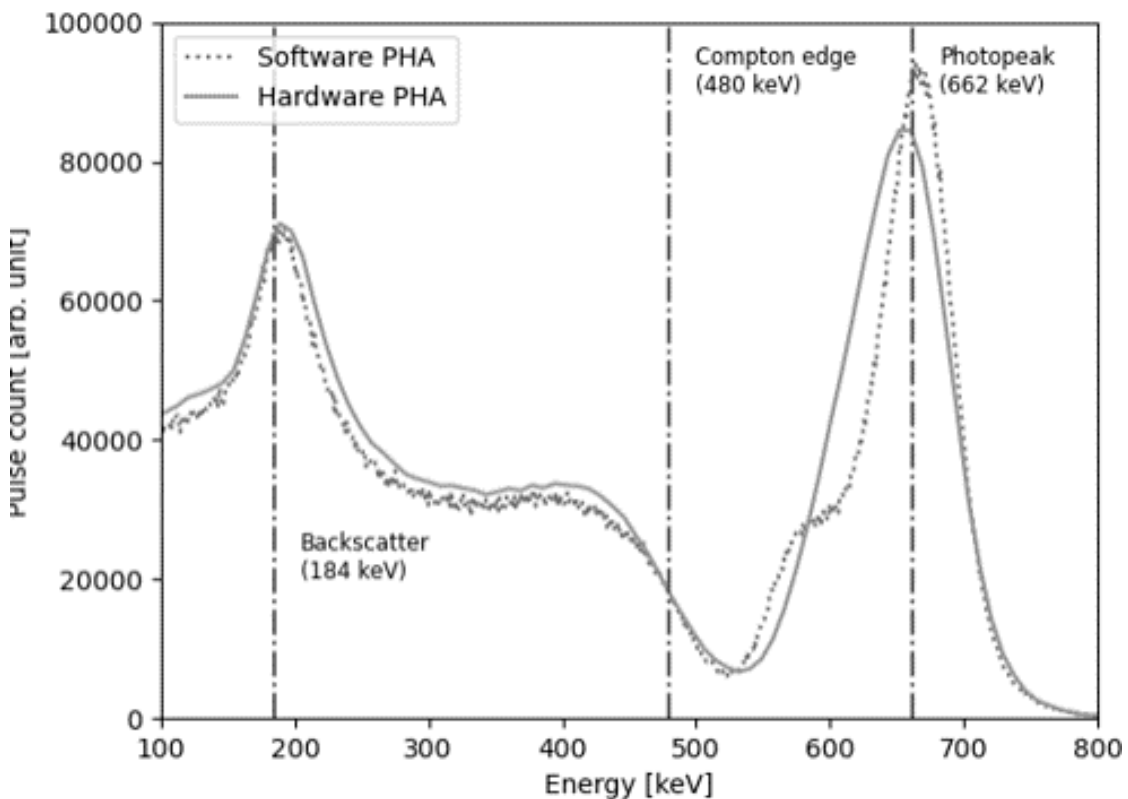


Figure 33: Spectrum obtained with the developed HXRM module

6.5 Spectrum storage and transfer

The HXRM specification requires it to operate in continuous windowed mode. Spectras are collected in 10 ms windows. As soon as one window finishes, the device should start creating a second spectrum, while simultaneously transferring the first one to the PC. No dead-time should occur when starting a new sampling window.

This requirement poses a problem when it comes to the spectrum storage. With 14-bit

samples the maximum theoretical resolution of the spectrum that can be obtained is also going to be 14 bits. A spectrum is essentially an array of pulse counts in each bin range. With 32 bits chosen for the count resolution a total of 2^{14} 32-bit words is required to store a single spectrum. This requires the use of Block Random Access Memory (BRAM) as no other FPGA structure can realize individually addressable increments on this scale within the timing constraints.

To prevent dead-time two BRAMs are used in an alternating mode. While one of the BRAMs is used to build the spectrum, the other one transfers its data to the PC and then resets its counts to back to zero. Figure 34 shows the schematic view of this idea. For long spectrum acquisition and debugging purposes an additional third BRAM is used. This memory is always incremented and can be read and reset using ADQ14's user registers.

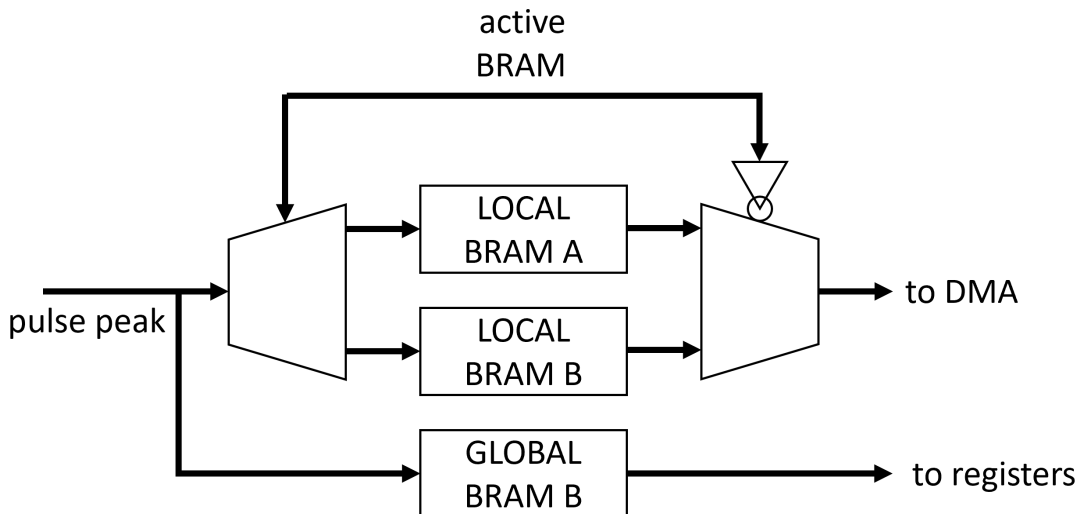


Figure 34: Spectrum storage with three BRAMs

The transfer and reset process requires the entire BRAM to be travelled twice. The ADQ14 can transfer 4 ADC samples or 64-bits of data on each FPGA clock cycle for each channel to the internal FIFO RAM. With 32-bit spectrum counts this makes it possible to transfer two bin counts on each clock cycle. To achieve that both port interfaces have to be used to read two bins next to each other. This in turn requires the BRAM to be travelled once again after transferring to reset all the count values to zero. This time both port interfaces are writing zeros to two consecutive addresses. With a 4 ns clock period the BRAM needs $33\mu s$ to transfer its contents and another $33\mu s$ to reset itself.

7 Data transfer

7.1 PCIe interface

7.2 Direct memory access

7.3 Data pathways in the system

7.4 Multi-threaded data transfer

7.5 Software optimization

8 Conclusions

8.1 Further problems

8.2 Future research

References

- [1] Stuart Kirsch. „Running out? Rethinking resource depletion”. In: *The Extractive Industries and Society* 7.3 (2020), pp. 838–840. ISSN: 2214-790X. DOI: <https://doi.org/10.1016/j.exis.2020.06.002>. URL: <https://www.sciencedirect.com/science/article/pii/S2214790X20301829>.
- [2] D.H. Meadows et al. *The Limits to Growth: A Report for the Club of Rome's Project on the Predicament of Mankind.* (A Signet classic) pkt 1. Universe Books, 1972. ISBN: 9780876631652. URL: https://books.google.pl/books?id=w%5C_9dAAAAIAAJ.
- [3] Steve Sorrell et al. „Shaping the global oil peak: A review of the evidence on field sizes, reserve growth, decline rates and depletion rates”. In: *Energy* 37.1 (2012). 7th Biennial International Workshop “Advances in Energy Studies”, pp. 709–724. ISSN: 0360-5442. DOI: <https://doi.org/10.1016/j.energy.2011.10.010>. URL: <https://www.sciencedirect.com/science/article/pii/S0360544211006694>.
- [4] IPCC et al. *Global warming of 1.5°C. An IPCC Special Report on the impacts of global warming of 1.5°C above pre-industrial levels and related global greenhouse gas emission pathways, in the context of strengthening the global response to the threat of climate change, sustainable development, and efforts to eradicate poverty.* Dec. 2018. ISBN: 9781009157957. DOI: 10.1017/9781009157940.
- [5] Alexey Mikhaylov et al. „Global climate change and greenhouse effect”. In: *Entrepreneurship and Sustainability Issues* 7.4 (2020), p. 2897.
- [6] Ibrahim Dincer. „Renewable energy and sustainable development: a crucial review”. In: *Renewable and Sustainable Energy Reviews* 4.2 (2000), pp. 157–175. ISSN: 1364-0321. DOI: [https://doi.org/10.1016/S1364-0321\(99\)00011-8](https://doi.org/10.1016/S1364-0321(99)00011-8). URL: <https://www.sciencedirect.com/science/article/pii/S1364032199000118>.
- [7] Ted Trainer. „Some problems in storing renewable energy”. In: *Energy Policy* 110 (2017), pp. 386–393. ISSN: 0301-4215. DOI: <https://doi.org/10.1016/j.enpol.2017.07.061>. URL: <https://www.sciencedirect.com/science/article/pii/S0301421517304925>.
- [8] Siddharth Suman. „Hybrid nuclear-renewable energy systems: A review”. In: *Journal of Cleaner Production* 181 (2018), pp. 166–177. ISSN: 0959-6526. DOI: <https://doi.org/10.1016/j.jclepro.2018.01.262>. URL: <https://www.sciencedirect.com/science/article/pii/S0959652618302993>.
- [9] Jack E. Fergusson. „The history of the discovery of nuclear fission”. In: *Foundations of Chemistry* 13.2 (July 2011), p. 145. ISSN: 1572-8463. DOI: 10.1007/s10698-011-9112-2. URL: <https://doi.org/10.1007/s10698-011-9112-2>.

- [10] Michael Dittmar. „Nuclear energy: Status and future limitations”. In: *Energy* 37.1 (2012). 7th Biennial International Workshop “Advances in Energy Studies”, pp. 35–40. ISSN: 0360-5442. doi: <https://doi.org/10.1016/j.energy.2011.05.040>. URL: <https://www.sciencedirect.com/science/article/pii/S0360544211003653>.
- [11] *Advanced Nuclear Reactors: Technology Overview and Current Issues*. Government Report. Congressional Research Service, 2019. URL: <https://crsreports.congress.gov/product/pdf/R/R45706>.
- [12] Steven J. Zinkle and Jeremy T. Busby. „Structural materials for fission & fusion energy”. In: *Materials Today* 12.11 (2009), pp. 12–19. ISSN: 1369-7021. doi: [https://doi.org/10.1016/S1369-7021\(09\)70294-9](https://doi.org/10.1016/S1369-7021(09)70294-9). URL: <https://www.sciencedirect.com/science/article/pii/S1369702109702949>.
- [13] Jef Ongena and Yuichi Ogawa. „Nuclear fusion: Status report and future prospects”. In: *Energy Policy* 96 (2016), pp. 770–778. ISSN: 0301-4215. doi: <https://doi.org/10.1016/j.enpol.2016.05.037>. URL: <https://www.sciencedirect.com/science/article/pii/S0301421516302658>.
- [14] Daniel Clery. „Fusion power may run out of fuel before it even gets started”. In: *Science* 376 (June 2022). doi: 10.1126/science.add5489.
- [15] Matteo Barbarino. „A brief history of nuclear fusion”. In: *Nature Physics* 16.9 (Sept. 2020), pp. 890–893. ISSN: 1745-2481. doi: 10.1038/s41567-020-0940-7. URL: <https://doi.org/10.1038/s41567-020-0940-7>.
- [16] ITER. *ITER - the way to new energy*. <https://www.iter.org/>. [Online; accessed 22-July-2022].
- [17] *Wendelstein 7-X / Max-Planck-Institut für Plasmaphysik*. <https://www.ipp.mpg.de/w7x>. [Online; accessed 22-July-2022].
- [18] Elizabeth Gibney. „Nuclear-fusion reactor smashes energy record”. en. In: *Nature* 602.7897 (Feb. 2022), p. 371.
- [19] ITER. *On the road to ITER: milestones*. <https://www.iter.org/proj/itermilestones>. [Online; accessed 22-July-2022].
- [20] Daniel Clery and Adrian Cho. „More Delays for ITER, as Partners Balk at Costs”. en. In: *Science* 352.6286 (May 2016), pp. 636–637.
- [21] ITER. *Diagnostics*. <https://www.iter.org/mach/Diagnostics>. [Online; accessed 22-July-2022].
- [22] Pat Brans. *Archiving 20 Gigabytes per Second and Making it Usable*. <https://www.iter.org/newsline/-/3585>. [Online; accessed 22-July-2022].
- [23] ITER. *Ensuring real-time distributed computing at ITER*. <https://www.iter.org/newsline/-/3599>. [Online; accessed 22-July-2022].

- [24] Xilinx. *What is an FPGA? Field Programmable Gate Array*. <https://www.xilinx.com/products/silicon-devices/fpga/what-is-an-fpga.html>. [Online; accessed 23-July-2022].
- [25] Patryk Nowak vel Nowakowski, Dariusz Makowski, and Aleksander Mielczarek. „Low-noise Amplifier for Photomultiplier Tube Detectors for Plasma Diagnostics”. In: *2021 28th International Conference on Mixed Design of Integrated Circuits and System*. 2021, pp. 69–73. doi: 10.23919/MIXDES52406.2021.9497532.
- [26] ITER. *Generating runaway electrons in JET to benefit ITER*. <https://www.iter.org/newsline/-/2234>. [Online; accessed 22-July-2022].
- [27] Gerardo D'Elia et al. „Preliminary study of a fast massive gas injection system for plasma disruption mitigation”. In: *Journal of Vacuum Science & Technology B* 36.1 (2018), 01A103. doi: 10.1116/1.4996069. eprint: <https://doi.org/10.1116/1.4996069>. URL: <https://doi.org/10.1116/1.4996069>.
- [28] V V Plyusnin et al. „Hard X-ray bremsstrahlung of relativistic runaway electrons in JET”. In: *J. Instrum.* 14.09 (Sept. 2019), pp. C09042–C09042. doi: <https://doi.org/10.1088/1748-0221/14/09/C09042>.
- [29] M.J. Pelletier and C.C. Pelletier. „RAMAN SPECTROSCOPY | Instrumentation”. In: *Encyclopedia of Analytical Science (Second Edition)*. Ed. by Paul Worsfold, Alan Townshend, and Colin Poole. Second Edition. Oxford: Elsevier, 2005, pp. 94–104. ISBN: 978-0-12-369397-6. doi: <https://doi.org/10.1016/B0-12-369397-7/00529-X>. URL: <https://www.sciencedirect.com/science/article/pii/B012369397700529X>.
- [30] Elisabete Freitas et al. „PMT calibration of a scintillation detector using primary scintillation”. In: *Journal of Instrumentation* 10 (Feb. 2015), pp. C02039–C02039. doi: 10.1088/1748-0221/10/02/C02039.
- [31] A.G. Wright. *Why Photomultipliers Need Amplifiers*. https://www.photonics.com/Articles/Why_PhotoMultipliers_Need_Amplifiers/a14120. [Online; accessed 23-July-2022].
- [32] G. Ripamonti, A. Pullia, and A. Geraci. „Digital vs. analogue spectroscopy: a comparative analysis”. In: *IMTC/98 Conference Proceedings. IEEE Instrumentation and Measurement Technology Conference. Where Instrumentation is Going (Cat. No.98CH36222)*. Vol. 1. 1998, 666–669 vol.1. doi: 10.1109/IMTC.1998.679876.
- [33] Esther Rani Thuraka et al. „Digital Multi-Channel analyzer for detection and analysis of radiation in nuclear spectroscopy”. In: *Materials Today: Proceedings* 38 (2021). International Conference & Exposition on Mechanical, Material and Manufacturing Technology (ICE3MT), pp. 3160–3167. ISSN: 2214-7853. doi: <https://doi.org/10.1016/j.matpr.2020.09.580>. URL: <https://www.sciencedirect.com/science/article/pii/S2214785320372965>.

- [34] Wojciech Walewski, Patryk Nowak Vel Nowakowski, and Dariusz Makowski. „Giga-sample Pulse Acquisition and Digital Processing for Photomultiplier Detectors”. In: *Journal of Fusion Energy* 41 (June 2022). doi: 10.1007/s10894-022-00320-0.
- [35] Jong-Gu Kwak et al. „KSTAR Status and Upgrade Plan Toward Fusion Reactor”. In: *IEEE Transactions on Plasma Science* 48.6 (2020), pp. 1388–1395. doi: 10.1109/TPS.2020.2964776.
- [36] R. O'Connor, J. Kadi, and S. Pandya. *System Design Description (DDD) 55.EE Hard X-Ray Monitor (H/He-Phase)*. Tech. rep. May 2021.
- [37] Patryk Nowak vel Nowakowski, Dariusz Makowski, and Wojciech Walewski. *PMT Signal Transmission for Hard X-Ray Diagnostics of Future Tokamaks*. 2022. doi: 10.21203/rs.3.rs-1529765/v1. URL: <https://doi.org/10.21203/rs.3.rs-1529765/v1>.
- [38] A. Georgiev, W. Gast, and R.M. Lieder. „An analog-to-digital conversion based on a moving window deconvolution”. In: *IEEE Transactions on Nuclear Science* 41.4 (1994), pp. 1116–1124. doi: 10.1109/23.322868.
- [39] Muhammad Faisal et al. „A correlation-based pulse detection technique for gamma-ray/neutron detectors”. In: *Nuclear Instruments and Methods in Physics Research Section A: Accelerators, Spectrometers, Detectors and Associated Equipment* 652.1 (2011). Symposium on Radiation Measurements and Applications (SORMA) XII 2010, pp. 479–482. ISSN: 0168-9002. DOI: <https://doi.org/10.1016/j.nima.2010.10.072>. URL: <https://www.sciencedirect.com/science/article/pii/S016890021002334X>.
- [40] J. Kamleitner et al. „Comparative analysis of digital pulse processing methods at high count rates”. In: *Nuclear Instruments and Methods in Physics Research Section A: Accelerators, Spectrometers, Detectors and Associated Equipment* 736 (2014), pp. 88–98. ISSN: 0168-9002. DOI: <https://doi.org/10.1016/j.nima.2013.10.023>. URL: <https://www.sciencedirect.com/science/article/pii/S0168900213013697>.
- [41] Mohammad-Reza Mohammadian-Behbahani and Shahyar Saramad. „A comparison study of the pile-up correction algorithms”. In: *Nuclear Instruments and Methods in Physics Research Section A: Accelerators, Spectrometers, Detectors and Associated Equipment* 951 (2020), p. 163013. ISSN: 0168-9002. DOI: <https://doi.org/10.1016/j.nima.2019.163013>. URL: <https://www.sciencedirect.com/science/article/pii/S0168900219313804>.
- [42] Valentin T. Jordanov et al. „Digital techniques for real-time pulse shaping in radiation measurements”. In: *Nuclear Instruments and Methods in Physics Research Section A: Accelerators, Spectrometers, Detectors and Associated Equipment* 353.1 (1994), pp. 261–264. ISSN: 0168-9002. doi: [https://doi.org/10.1016/0168-9002\(94\)91652-7](https://doi.org/10.1016/0168-9002(94)91652-7). URL: <https://www.sciencedirect.com/science/article/pii/0168900294916527>.